Please cite this article in press as: Bai et al., Theory and applications of high-voltage triboelectric nanogenerators, Cell Reports Physical Science (2022), https://doi.org/10.1016/j.xcrp.2022.101108

Cell Reports
Physical Science

CellPress
OPEN ACCESS

Review

Theory and applications of high-voltage triboelectric nanogenerators

Yuan Bai,[1,2] Hongqing Feng,[1,3,*] and Zhou Li[1,2,3,*]

SUMMARY

As an emerging energy-harvesting technology, triboelectric nanogenerators (TENGs) have made rapid progress in the past decade. Alongside the well-known self-powering behavior, TENGs also have another unique feature: high-voltage and low-current output. It is relatively easy for TENGs to achieve voltage outputs of hundreds and even thousands of volts, while the current output remains on the order of several micro-amperes. This brings opportunities to develop safe high-voltage applications. This review introduces the fundamental theories of voltage generation by TENGs and summarizes the strategies to boost TENG voltage up to tens of kilovolts. The applications of these high-voltage TENGs (HV-TENGs) in physical, chemical, and biological fields are also reviewed in detail. Finally, the opportunities and challenges for HV-TENGs are discussed.

INTRODUCTION

With the impending energy crisis, alternatives to fossil fuels are urgently demanded. Various energy-harvesting technologies based on electromagnetic,[1,2] photovoltaic,[3–5] thermoelectric,[6,7] piezoelectric,[8–10] and triboelectricity[11–15] principles, have been rapidly developed. Among them, triboelectric nanogenerators (TENGs), which can convert mechanical energy into electrical energy, have received significant attention from researchers in recent years. TENGs have been extensively studied in wind energy,[16–18] ocean energy,[19–21] vibration energy,[22,23] and droplet energy[24–26] collection. Meanwhile, the human body is also a rich energy source. TENGs cannot only collect the large movement energy to power wearable electronic devices,[27–29] but also collect the subtle mechanical energy produced by life activities, such as heartbeat[30,31] and breathing,[32–34] to power implanted medical electronic devices for disease treatment and monitoring. Compared with other energy-harvesting technologies, TENGs have demonstrated the advantages of wide material sources, low cost, simple structure, and high energy conversion efficiency.

High voltage has been widely applied in particle accelerators,[35,36] high-power pulse generators,[37,38] electrostatic control and protection,[39,40] laser technology,[41,42] plasma,[43,44] and many other fields.[45,46] However, traditional high-voltage sources have disadvantages of high power consumption, dependency on the power grid, and safety concerns. TENGs possessing a high internal resistance are emerging as an ideal high-voltage source. Their voltage can easily reach hundreds of volts, even tens of kilovolts sometimes, but their currents are at the scale of microamperes.[47,48] Compared with commercial high-voltage sources, high-voltage TENGs (HV-TENGs) have the advantages of high safety, low energy consumption, and no requirement for an external power supply.

[1]Beijing Key Laboratory of Micro-nano Energy and Sensor, Beijing Institute of Nanoenergy and Nanosystems, Chinese Academy of Sciences, Beijing 101400, China

[2]Center on Nanoenergy Research, School of Physical Science and Technology, Guangxi University, Nanning 530004, China

[3]School of Nanoscience and Technology, University of Chinese Academy of Sciences, Beijing 100049, China

*Correspondence:
fenghongqing@binn.cas.cn (H.F.),
zli@binn.cas.cn (Z.L.)

https://doi.org/10.1016/j.xcrp.2022.101108

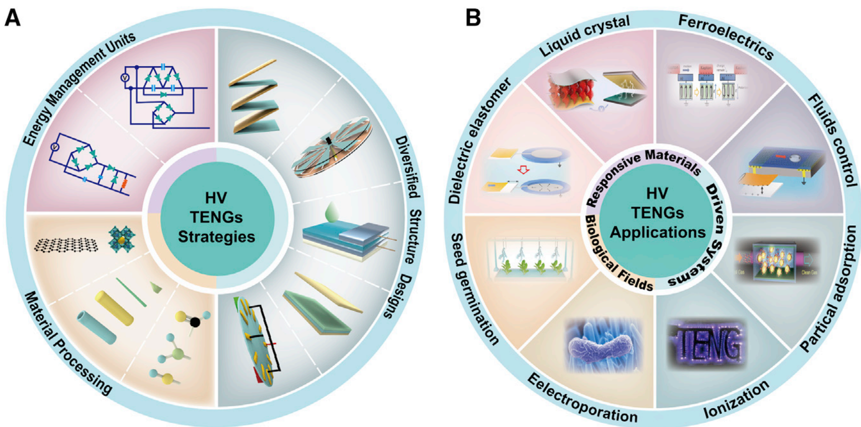

Figure 1. Summary of the output boosting strategies and featured applications for HV-TENGs
(A) Output boosting and (B) applications.

In this review, we first give a brief introduction of the fundamental theories of TENGs generating high voltage. Based on the affecting factors, the strategies that can elevate the TENGs voltages to thousands of volts are reviewed, from structural designs to energy management units, as shown in Figure 1A. Next, we summarize the featured applications of HV-TENGs in the electrically responsive materials, micro-driven systems, and biological fields, as shown in Figure 1B. In the end, the challenges and future development of HV-TENGs are proposed.

THEORY OF TENGs VOLTAGE OUTPUT

The fundamental theory of TENGs comes from Maxwell's displacement current.[49,50] The displacement current is due to the time-varying electric field coupled with the time-varying tiny movements of atomic bound charges and the polarization of the dielectric in the material. In a dielectric with surface polarization charges, the displacement current is contributed by the polarization density Ps.

$$J_D = \frac{\partial D}{\partial t} = \varepsilon \frac{\partial E}{\partial t} + \frac{\partial P_S}{\partial t} \quad \text{(Equation 1)}$$

Here, J_D represents the displacement current, D represents the displacement field, ϵ represents the dielectric constant, and E represents the electric field. The second term is the current caused by the polarization field generated by the electrostatic charges on the surface. There are four operating modes in TENGs (Figure 2), and we will introduce the open circuit voltage (V_{OC}) formulas for each of them.

Contact-separation mode

In the contact-separation mode, two different films with back electrodes are stacked face to face. The two films get positive and negative charges during the contact process, respectively. At the same time, opposite charges corresponding to the film are induced on each back electrode. Once separated, a potential difference between the two electrodes will come out. The V_{OC} can be expressed as[51,52]:

$$V_{OC} = \frac{\sigma x(t)}{\varepsilon_0}. \quad \text{(Equation 2)}$$

Here, σ represents charge density, x represents separation displacement, and ϵ_0 represents vacuum dielectric constant.

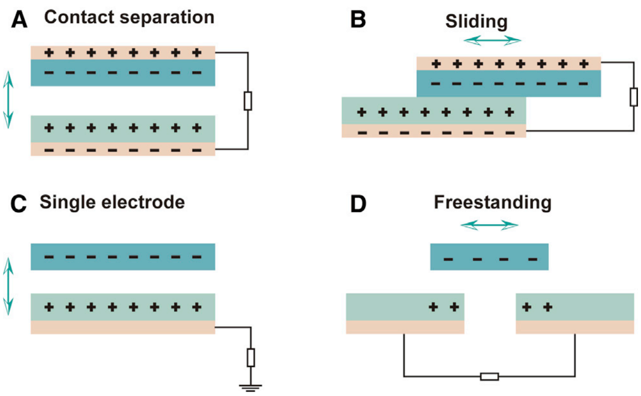

Figure 2. Four classical modes of TENGs
(A) Contact-separation mode.
(B) Sliding mode.
(C) Single-electrode mode.
(D) Freestanding mode.

Sliding mode

In the sliding mode, the two different films with the back electrodes overlap completely at the beginning. Due to the different ability to gain and lose electrons, they are charged with positive and negative charges, respectively. Once it starts to slide outward, the contact area between the two materials decreases, resulting in the separation of charges in the plane and generating a potential difference. The V_{OC} can be expressed as[53]:

$$V_{OC} = \frac{\sigma x d_0}{\varepsilon_0 (l - x)}. \quad \text{(Equation 3)}$$

Here, σ represents charge density, d_0 represents effective thickness constant, x represents horizontal sliding displacement, ϵ_0 represents vacuum dielectric constant, and l represents board length.

Single-electrode mode

The single-electrode mode is different from the above two modes in that one electrode is connected to the back electrode of the triboelectric material and the other electrode is grounded as a reference electrode. Therefore, the other triboelectric layer of the single-electrode mode TENGs is not restricted by the electrode and can be a freely moving object. Due to the electrostatic shielding effect of the main electrode, its output is half that of the dual-electrode TENG.[54]

When l approaches 0, x / l and g / l is very large,

$$V_{OC} = \frac{\sigma}{2\varepsilon_0}\pi l. \quad \text{(Equation 4)}$$

When l approaches infinity, x / l and g / l is close to 0,

$$V_{OC} = \frac{\sigma g x \ln l}{\pi \varepsilon_0 l}, \quad \text{(Equation 5)}$$

here, σ represents charge density, x represents the gap between the two triboelectric materials, ϵ_0 represents vacuum dielectric constant, l represents board length, and g represents gap between the main electrode and reference electrode.

Freestanding mode

An independent layer of the same size exists on two parallel electrodes, which may or may not be in contact with the electrodes. Since the independent layer itself possesses some charge, an opposite charge will be induced on the corresponding electrode. The potential difference is generated when the independent layer has moved from one electrode to the other.[55]

$$V_{OC} = \frac{2Nd\theta_0\sigma\alpha\left(r_2^2 - r_1^1\right)}{N\varepsilon_0\varepsilon_r\alpha(\theta_0 - \alpha)\left(r_2^2 - r_1^1\right) + 2d\theta_0 C_p}, \quad 0 \le \alpha \le \theta_0$$
$$V_{OC} = \frac{2Nd\theta_0\sigma(2\theta_0 - \alpha)\left(r_2^2 - r_1^1\right)}{N\varepsilon_0\varepsilon_r(\alpha - \theta_0)(2\theta_0 - \alpha)\left(r_2^2 - r_1^1\right) + 2d\theta_0 C_p}, \quad \theta_0 \le \alpha \le 2\theta_0 \quad \text{(Equation 6)}$$

Here, σ represents charge density, d represents thickness, N represents number of grating units, θ_0 represents center angle of grating units, α represents rotation angle, ϵ_0 and ϵ_r represent the permittivity of vacuum and relative permittivity of dielectrics, C_p represents the parasitic capacitance between electrodes, r_1, r_2 represents inner and outer radius, respectively.

Despite the four different modes, the V_{OC} is all proportional to the surface charge density σ according to Equations (2–6). Therefore, increasing the surface charge density of the device is significant for increasing TENGs output. In the next section, we introduce the effective strategies to increase TENGs output.

STRATEGIES TO FABRICATE HV-TENG

Overview of the reported HV-TENGs

Theoretical calculations have shown that the V_{OC} of TENGs is positively correlated with the surface charge density σ. The TENGs are based on the coupling effect of contact electrification and electrostatic induction.[12] Contact electrification means that, when two different materials are in contact, the two material surfaces will be charged with positive and negative charges, respectively. The charge amount depends on the ability of these two materials to gain or lose electrons. Therefore, choosing the appropriate materials and material processing methods is an efficient strategy to enhance the surface charge density. This includes physical surface topography processing,[56–58] surface chemical modification,[59–62] and composite materials with adjusted dielectric constants.[63] Surface morphology processing is a relatively simple, efficient, and rapid method to increase the TENGs' surface charge density. Researchers have produced micro-nano structures including nanowires,[64] nanopillars,[65,66] nanotubes,[67] porous,[68,69] and even some natural micro-nano patterns on the surface of triboelectric materials.[57,70–73] The difference in the ability of materials to gain or lose electrons stems from the different functional groups on the surface of the material. The modification of the functional groups on the surface of the material endows the material with a stronger ability to gain and lose electrons without changing the basic properties.[59,62] For example, adding high permittivity materials to the polymer reveals a strong internal polarization under the action of triboelectric charges, enhancing the induction capability of the bottom electrode charge.[74] A fluorine-modified polypropylene TENG with nanowire arrays generated a maximum V_{OC} of 1,900 V.[75] In recent years, some emerging materials have attracted the attention of researchers as functional doping materials, such as graphene,[76,77] MXenes,[78,79] black phosphorus,[80,81] metal-organic frameworks,[82,83] hexagonal boron nitride,[63] and perovskite materials.[84,85] Kim et al. doped $CaCu_3Ti_4O_{12}$ (CCTO) with high permittivity particles (the permittivity constant of CCTO is as high as 7,500) into polymer butylmelamine formaldehyde (BMF) as triboelectric materials.[74] The voltage of the BMF-CCTO-TENG reached about 450 V, which was 3-fold that of the pure BMF-TENG. Doping the high dielectric constant carbon dots enhanced the interface polarization and surface charge density, the polyethylenimine (PEI) functionalized N-doped carbon dots PEI-based TENGs revealed a remarkable

Please cite this article in press as: Bai et al., Theory and applications of high-voltage triboelectric nanogenerators, Cell Reports Physical Science (2022), https://doi.org/10.1016/j.xcrp.2022.101108

Table 1. Summary of >2 kV TENGs

Modes	Triboelectric materials	Size (mm)	Voltage (kV)	Application	Reference
CS-TENG (contact-separation TENG)	PTFE, Al	85 × 105	7	electro-adhesion	Xu et al.[90]
	PU, ebonite	100 × 100	2.2	ammonia synthesis	Wong et al.[91]
	PTFE, Cu	70 × 70	2	negative air ion generator	Guo et al.[92]
	PTFE, Al	67 × 55	16.5	lighting up LEDs	Wang et al.[93]
	PTFE, Al	100 × 100	7.5	lighting up LEDs	Wang et al.[94]
	Kapton, Al	100 × 100	3.6	optical modulator	Chen et al.[95]
	PVDF, nylon	50 × 50	2.8	water/oil separation	Yang et al.[96]
FR-TENG (freestanding rotary TENG)	Kapton, nylon	Φ: 230	20	oil purification	Lei et al.[47]
	PTFE, rabbit fur	Φ: 177	4.5	smart farming	Han et al.[97]
	PTFE, rabbit fur	Φ: 135	3.7	smart farming	Chen et al.[98]
	PTFE, nylon, polyester fur	Φ: 221	10	seed germination	Li et al.[99]
	PTFE, rabbit hair	Φ: 200	3	seed germination	Li et al.[100]
	PTFE, paper	Φ: 200	2.3	sterilization	Feng et al.[101]
	PET, FEP	Φ: 300	6.9	sterilization	Chen et al.[102]
	PTFE, nylon	Φ: 245	30.7	sterilization	Lei et al.[103]
	–	–	9.3	sterilization	Luo et al.[104]
	PTFE, paper	Φ: 260	3	CWA decontamination	Bai et al.[105]
	Kapton, Cu	Φ: 200	7	ammonia synthesis	Han et al.[106]
	Kapton, Cu	Φ: 200	2.5	ammonia synthesis	Han et al.[107]
	PTFE, Cu	Φ: 144	6	fog collection system	Gu et al.[108]
	Kapton, Cu	Φ: 220	3.2	lighting up LEDs	Bai et al.[109]
	PVC, nylon	Φ: 280	3.6	lighting up LEDs	Yang et al.[110]
	FEP, nylon	Φ: 128	3.6	lighting up LEDs	Fu et al.[111]
	Kapton, Al	–	3.4	driven droplet	Nie et al.[112]
	FEP, Cu	Φ: 300	8	electrospinning	Li et al.[113]
	PTFE, Al	140 × 90	3	vehicle exhaust treatment	Han et al.[114]
	PVC, nylon	Φ: 300	8	electro-assisted cell printing	Huo et al.[115]
FS-TENG (freestanding sliding TENG)	PTFE, Cu	185 × 185	3	triboelectric micromotor	Yang et al.[116]
	PTFE, Cu	240 × 100	2.2	MoS2 surface modulation	Zhao et al.[117]
	PTFE, Cu	150 × 120	5.3	artificial synapse	Zhang et al.[118]
	PTFE, nylon	80 × 60	6	lighting up LEDs	Shan et al.[119]
	PTFE, nylon	77.5 × 54	5	lighting up LEDs	He et al.[120]
	PTFE, PU	150 × 100	35	micro-flow pump	Sun et al.[121]
	FEP, Cu	–	2	driving soft robot	Sun et al.[122]
	Kapton, Al	–	3	braille display system	Qu et al.[123]
	PTFE, nylon, Cu	–	5	driving droplet	Yu et al.[124]
	Kapton, Al	80 × 100	3.5	driven droplet	Nie et al.[125]

enhancement in power density of 28.5 times compared with pure TENGs.[86] Nevertheless, these common strategies have been described in detail in many reviewed literatures, and most related TENG outputs are not very high.[87–89] In this review, we focus on the HV-TENGs that are capable of generating outputs up to thousands of volts.

We summarize the reported HV-TENGs with an output voltage of over 2 kV, and the results are shown in Table 1 and Figure 3. Freestanding rotary TENG (FR-TENG) is the most dominant type to achieve high voltage, which holds the highest ratio (54.1%) among all the studied TENGs (Figure 3A). There are two reasons for this. One is that the high rotary frequency of FR-TENG is very helpful in generating high voltage. Meanwhile, the FR-TENG possesses more complex structure designs that allow functionalization from many aspects. According to Equation 1, the structure involves more parameters (N, θ_0, r_1, r_2), which provides more possibilities for output

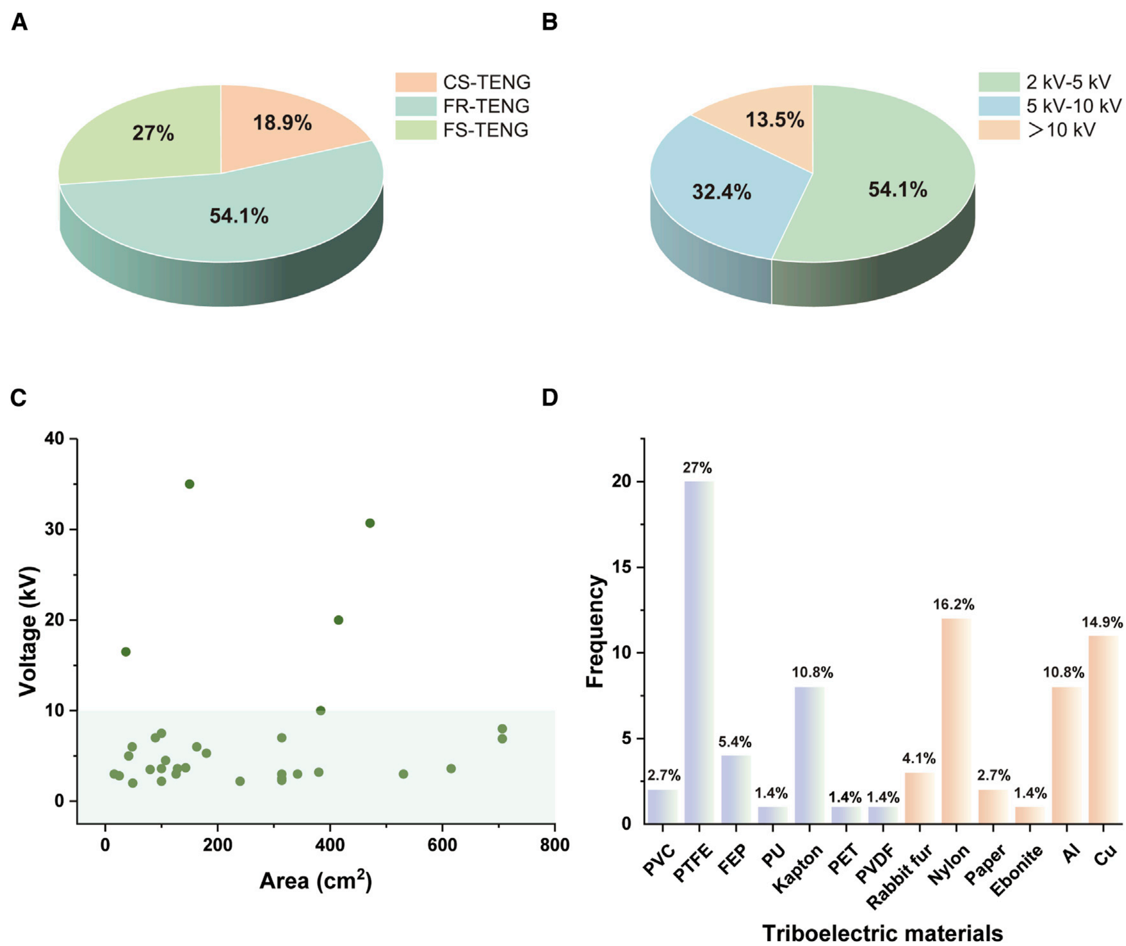

Figure 3. Statistics of the over 2 kV HV-TENGs
(A) The ratio of different TENGs types.
(B) The ratio of different output range.
(C) The dependence of the output on the triboelectric area.
(D) The use frequency of various triboelectric materials.

promotion. The freestanding sliding TENG (FS-TENG) takes a portion of 27% (Figure 3A). Referring to the output range, 86.5% of the output voltage is within 2–10 kV (54.1% + 32.4%), and only 13.5% of the studied TENGs are capable of generating a voltage higher than 10 kV, as shown in Figure 3B. The output is not highly related to the friction area. As shown in Figure 3C, the highest output 35 kV is generated by an FR-TENG with an area of only 150 cm^2. As for the fabrication materials, according to Figure 3D, PTFE and Kapton are the most frequently used negative triboelectric materials; nylon, Cu, and Al are the most frequently chosen positive materials. There are no special requirements on the materials for the HV-TENGs.

Based on the above survey, the HV-TENGs that achieve outputs of thousands of volts are not dependent on special materials or large friction area. Instead, the high-voltage outputs are mainly based on special structural designs and energy management, as discussed below.

Boosting strategies based on structural design

The triboelectric layer wear and the surface charge dissipation will seriously reduce the performance of TENGs. Flexible contact between triboelectric materials and

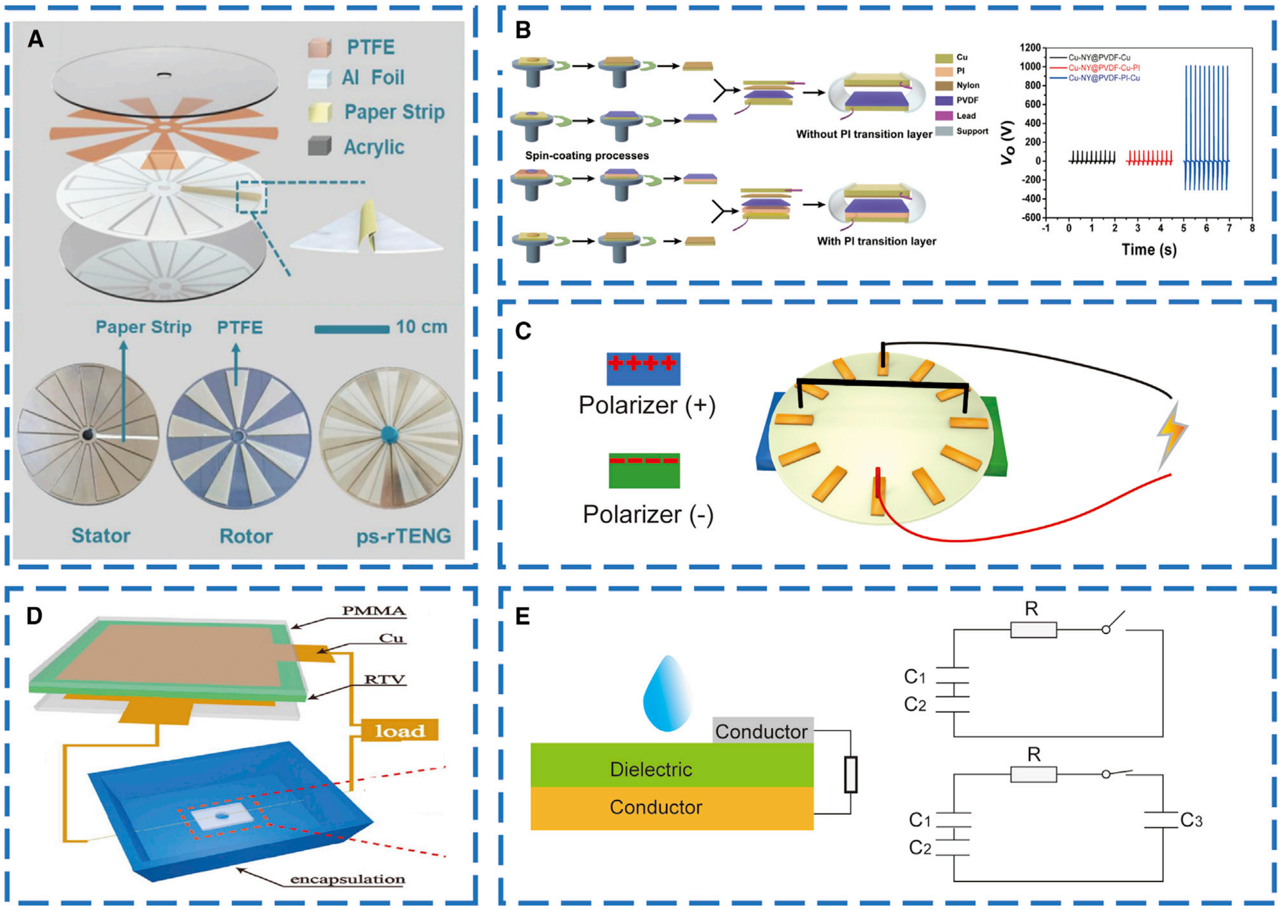

Figure 4. Structural designs of HV-TENGs to boost the output

(A) Continuous charge replenishment and flexible contact enabled by a paper strip for an FR-TENG.[101] Copyright 2021, Wiley-VCH.

(B) The PI intermediate layer acts as charge storage layer for a CS-TENG.[129] Copyright 2017, Elsevier.

(C) The charge accumulation strategy.

(D) The discharge switch for a CS-TENG.[130] Copyright 2018, Elsevier.

(E) Dual capacitor switching effect TENG.

continuous charge replenishment are important strategies to address the above problems.[21,97,98,126–128] As shown in Figure 4A, Feng et al. proposed an ultra-simple charge supplementary strategy for the FR-TENG.[101] They added a flexible paper strip (ps) between the rotor PTFE and the stator aluminum electrode pair as a charge replenishment source, continuously replenishing charge to the PTFE, and the new device is named ps-rTENG (Figure 4A). The V_{OC} of the ps-rTENG reached 2,352 V, which was triple the level of the conventional rTENG without the ps. Due to the flexible contact between the paper and PTFE, the V_{OC} hardly changed after 1,000k cycles.

In addition to the surface charge dissipating into the air, the electrons drift to the bottom electrode under the action of the electric field, which results in the recombination of the electrons with the induced positive charges, and the reduction of the surface charge density. Adding an intermediate layer between the triboelectric material and the electrode layer as a blocking layer or a charge storage layer can block the drift of surface electrons. Feng et al. added a 25-μm-thick Kapton (polyimide [PI]) film between the polyvinylidene difluoride (PVDF) and Cu electrodes as a charge storage layer for a CS-TENG.[129] As shown in Figure 4B, the fabricated TENG increased the V_{OC} from 110 V (without the PI interlayer) to 1,010 V. Besides polymers, the interlayers can be metal[131,132] or inorganic non-metallic.[133,134]

Lei et al. fabricated a HV-TENG using a charge accumulation structure.[47] The device consisted of a pair of polarizers (Kapton and nylon), a disk, a transmission bridge, and a pair of accumulators (Figure 4C). Two sets of electrodes with different functions were on the front and back of the disk. The back electrode (triboelectrode) was in contact with the polarizers to ensure the charge density of the polarizer dielectric layer remained saturated. The other set of electrodes (transporting electrodes) were connected to the transmission bridge for transferring the polarizer-induced charge to the accumulators. When the triboelectrodes contacted different polarizers, the polarizers were charged with positive and negative charges (negative for Kapton and positive for nylon). The transporting electrodes above the polarizers induced opposite charges. Under the strong electric field of the polarizer, the positive and negative charges accumulated on the transporting electrodes above the different polarizers through the transmission bridge, respectively. The continuously generated charges on the transporting electrodes accumulated on the accumulators, generating a high voltage of more than 20 kV at both ends of the accumulators.

In air, the breakdown phenomenon occurs when the electric field strength between two points is greater than the air breakdown strength (3 kV/mm). HV-TENGs, with output over 1 kV and triboelectric pairs in contact, often face breakdown problems. The breakdown will reduce the surface charge density and limit the output. To avoid the occurrence of breakdown, a vacuum environment is required.[135] But this is impractical in applications. Adding lubricating oil between the triboelectric pairs cannot only prevent the breakdown occurrence, but also reduce the wear, which is more suited for HV-TENGs.[136,137] Zhou et al. proposed adding liquid lubrication between the triboelectric layer and electrode for suppressing the interfacial electrostatic breakdown.[138] The maximum output power density of the lubricated sliding-mode TENG was enhanced by more than 50% (3.45 W m^{-2} Hz^{-1}). Chung et al. reported on a nonpolar large Debye length liquid lubricant submerged TENG to prevent electrostatic breakdown.[139] The combination with rolling friction significantly reduced the friction wear of the device. Meanwhile, the breakdown is accompanied with a high instantaneous current, and reasonable use of the breakdown in the external circuit can become a good output improvement strategy. Spark discharge can work as an efficient switch to control charges, offering very low leakage current and full-range voltage applicability.[94] As shown in Figure 4D, Zhai et al. proposed a spark discharge to improve the TENG performance.[130] When the voltage reached the noble gas breakdown voltage, a conductive path was formed between the needle-needle electrodes, releasing a large number of free charges. This device increased the peak-peak voltage from 300 to 1,300 V. Kim et al. constructed a TENG with sawtooth electrode creating a spark discharge in the gap between the serrated electrode and a wire. Based on the spark discharge, the designed secondary boost adapter achieved a high output voltage of 5 kV.[140]

Apart from the traditional solid-solid triboelectric layers, liquid-solid layers can also generate high voltage. Xu et al. constructed a simple water droplet energy collection device.[24] A PTFE film on an indium tin oxide substrate was coupled with an aluminum electrode for harvesting energy from the water droplets. The water droplets continuously dropped on the PTFE, and the charge density on the PTFE became saturated. Before the water droplet on the PTFE contacted the aluminum electrode, it was equivalent to the open switch. No capacitance was formed between the water and

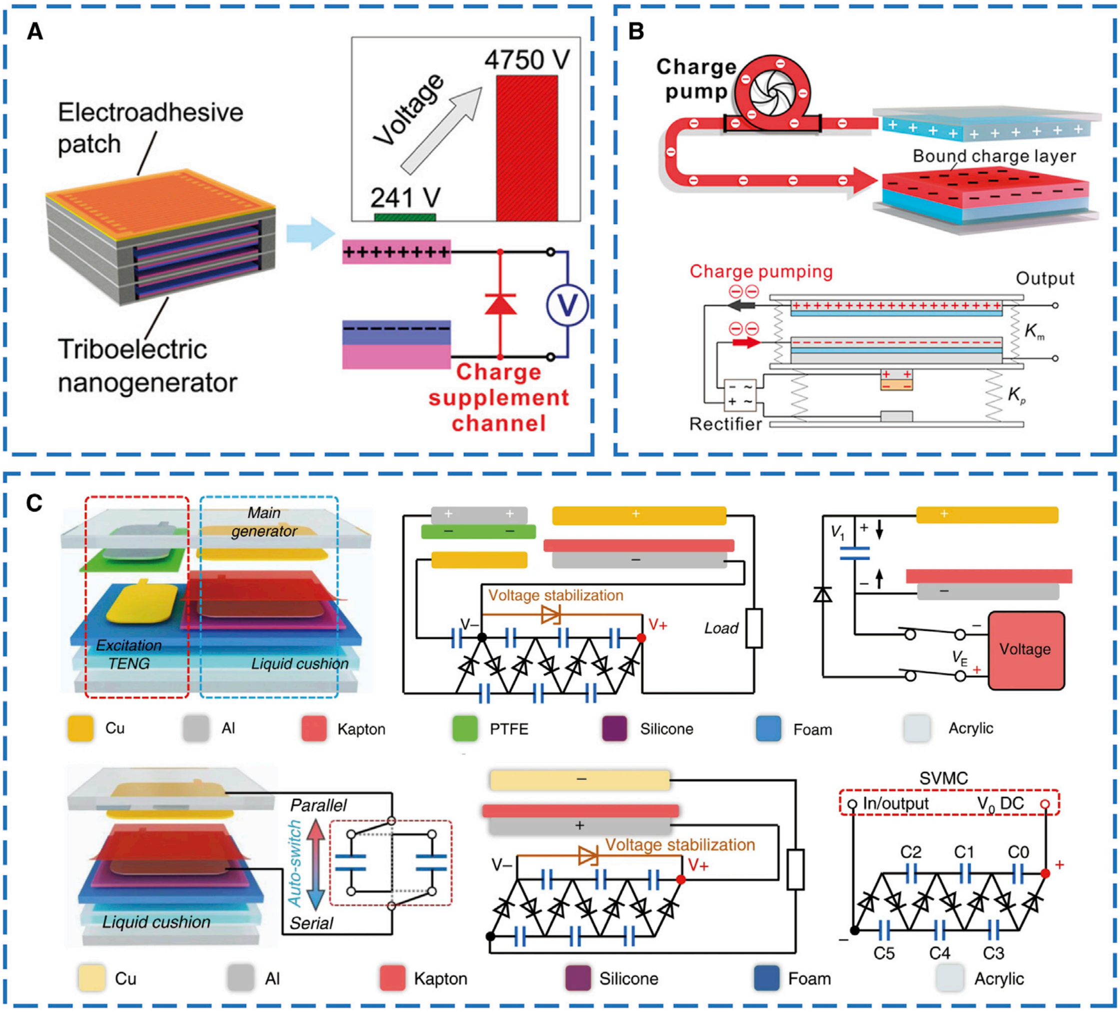

Figure 5. Energy management units for boosting the TENGs output

(A) A single diode acts as a charge supplement channel.[90] Copyright 2018, American Chemical Society.

(B) A charge pump help to elevate the output to severalfolds.[142] Copyright 2018, Elsevier.

(C) The VMC for external excitation and self-excitation of the TENGs.[146] Copyright 2019, Springer Nature.

the PTFE, and the charges could not be stored. Once the water was in contact with the aluminum electrode, the switch closed, and a capacitance formed. The mechanism is shown in Figure 4E. Combined with the high surface charge density on the PTFE, an instantaneously high voltage of 134.5 V was realized. Zhang et al. carried out a more in-depth study on this basis, a single water droplet output voltage reached 100 V without pre-charging.[141] Although the droplet collection device output voltage is well below 1,000 V, this design provides important inspiration for the HV-TENGs.

Boosting strategies based on energy management

Commercial electronic components exhibit a good effect on the TENG output regulation. As shown in Figure 5A, Xu et al. connected a single diode in the TENG as a charge replenishment channel to replenish the dissipated charge and achieved a significant 10-fold increase in the VOC from about 230 to 3,300 V.[90] They also designed a charge pump to boost the charge density of TENGs.[142] As shown in

Figure 5B, the charge pump consisted of the pump TENG and the main TENG. In this structure, the main TENG had one more metal floating layer than the pump TENG. The rectifier bridge rectified the charge in the pump TENG and transferred it unidirectionally to the metal floating layer. The metal floating layer can bind the electrons from the pump TENG to achieve a higher electron density. The main TENG achieved a peak voltage of 1,290 V and a surface charge density of 1,020 $\mu C\ m^{-2}$. Later, Bai et al. successfully applied this method to an FR-TENG. The peak-to-peak voltage reached 5.5 kV.[109] The diodes were connected in series, and the capacitors were connected in parallel between the two diodes to form a voltage multiplier circuit (VMC), which can multiply boost the output. Its working principle was to use diode rectification for charge storage in the same stage capacitor, charging the next stage capacitor, and finally achieving a multiplication. In recent years, it has been widely used for TENG performance improvement.[143–145] As shown in Figure 5C, Liu et al. achieved external excitation and self-excitation on the TENG using a VMC (triple multiplier: seven rectifier diodes, six ceramic capacitors) on the basis of the charge pump strategy.[146] A high surface charge density of 1.25 $mC\ m^{-2}$ and V_{OC} of 630 V were achieved.

FEATURED APPLICATIONS OF HV-TENGs

Application of HV-TENGs in electrically responsive materials

Dielectric elastomers are electrically actuated materials with low Young's modulus and large strain ability. Attaching two flexible electrodes to the upper and lower sides of a dielectric elastomer can form a dielectric elastomer actuator (DEA). When a strong electric field is applied, the opposite charges on the upper and lower electrodes generate electrostatic attraction, causing the dielectric elastomer to diminish in thickness and expand in area.[147] However, DEAs require a high voltage of several thousand volts. TENGs with high-voltage and low-current characteristics are an ideal high-voltage source. In recent years, TENGs-DEA has been applied to the fields of grating adjustment, soft robots, and disability assistance systems.[148,149]

As shown in Figure 6A, Chen et al. proposed a triboelectric tunable smart optical modulator (SOM).[95] The SOM consisted of a dielectric elastomer film and dispersed silver nanowire electrodes. The maximum output voltage of the constructed CS-TENG with a tribo-surface of 100 cm^2 reached 3.6 kV. The CS-TENG output reduced the SOM transmittance from 72% to 40% at contact-separation motion velocity ranging from 0.5 to 10 $cm\ s^{-1}$. Later, based on the above work, they investigated the strain period of a tunable optical grating driven by the CS-TENG.[150] By inducing dielectric elastomer grating deformation, The CS-TENG reduced the grating period by 16.5% or increased it by 9.4% when the contact surface was 120 cm^2. Stripe gratings, double-layer gratings, and lattice gratings were printed on elastomer films, and one-dimensional (1D) and 2D diffraction matrices were realized under the control of the TENG.

Soft robots have potential applications in biomedicine, underwater operations, and artificial assistance. DEAs are an emerging class of soft actuators with advantages of fast response, high energy density, and large strain. Combining TENGs with dielectric elastomers makes it possible to realize self-propelled soft robots. As shown in Figure 6B, Sun et al. developed a unidirectional DEA-driven soft robot combining an FS-TENG.[122] Its operating principle was that, when the FS-TENG slid back and forth, the charge accumulated and dissipated on the DEA, causing the DEA to stretch and shrink, and the one-way bearing wheel drove the soft robot to crawl in one direction. With a square wave voltage of 26 Hz and 4 kV applied, the robot

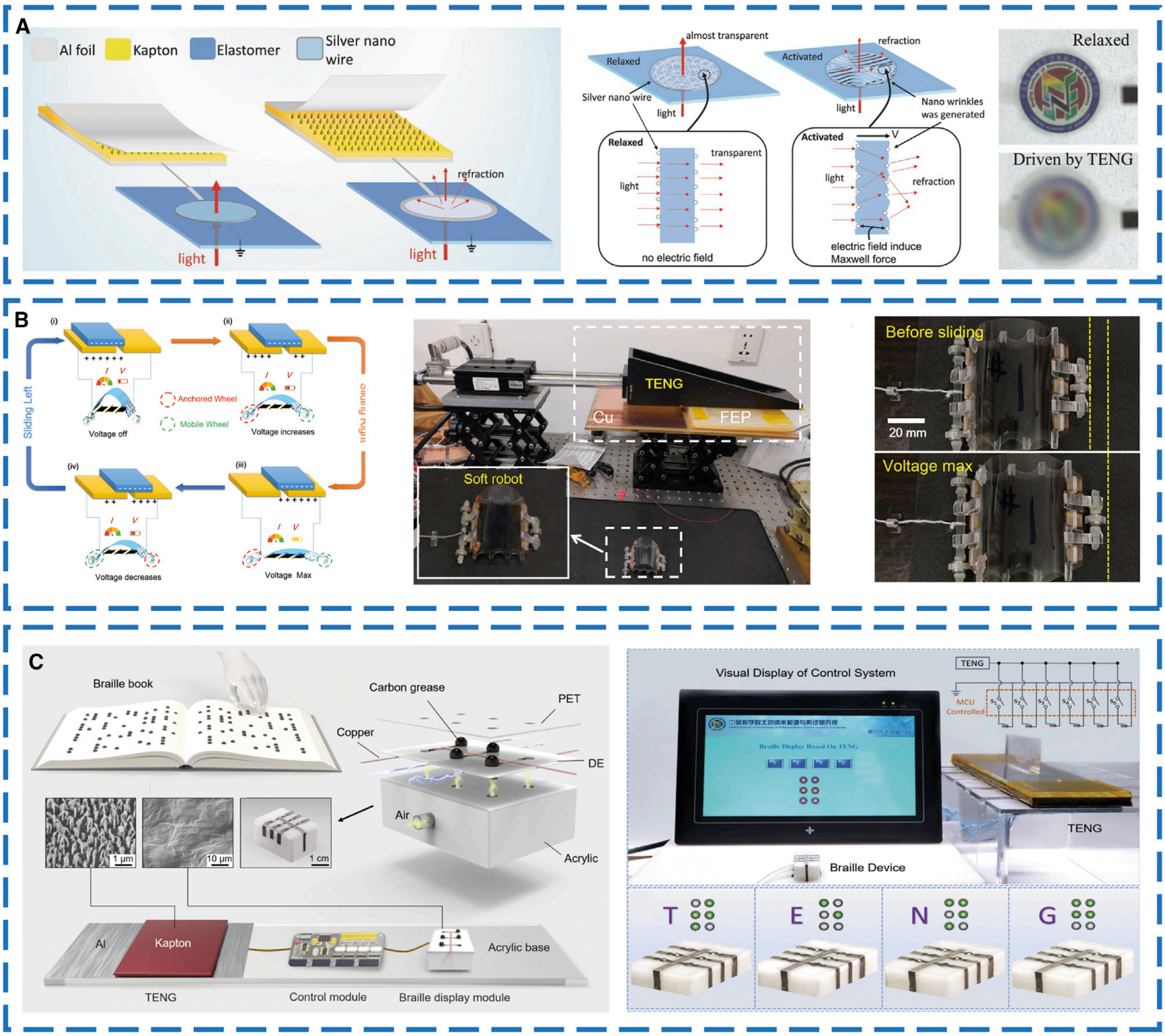

Figure 6. TENG-driven dielectric elastomers

(A) A CS-TENG-driven dielectric elastomer for grating adjustment.[95] Copyright 2016, Wiley-VCH.
(B) A DEA-driven soft robot combining an FS-TENG.[122] Copyright 2021, Elsevier.
(C) An FS-TENG-driven braille device.[123] Copyright 2020, Wiley-VCH.

demonstrated a maximum crawling speed of 110 mm (2.2 body-length) s^{-1} and a load capacity of 40 g. It opened up a new path for self-powered intelligent soft robots.

Braille devices made of dielectric elastomers are hoped to be refreshable, so that they can capture real-time information. As shown in Figure 6C, Qu et al. fabricated a triboelectrically driven braille device using an FS-TENG instead of a commercial power source.[123] The FS-TENG generated a voltage of more than 3 kV, resulting in dielectric elastomer deformation. Meanwhile, supported by the pressurized air in the chamber, the membrane was raised up to form a tactile braille dot. They designed a braille writing system with visual program control. Utilizing electronic switches, the display of different characters "T," "E," "N," and "G" was realized

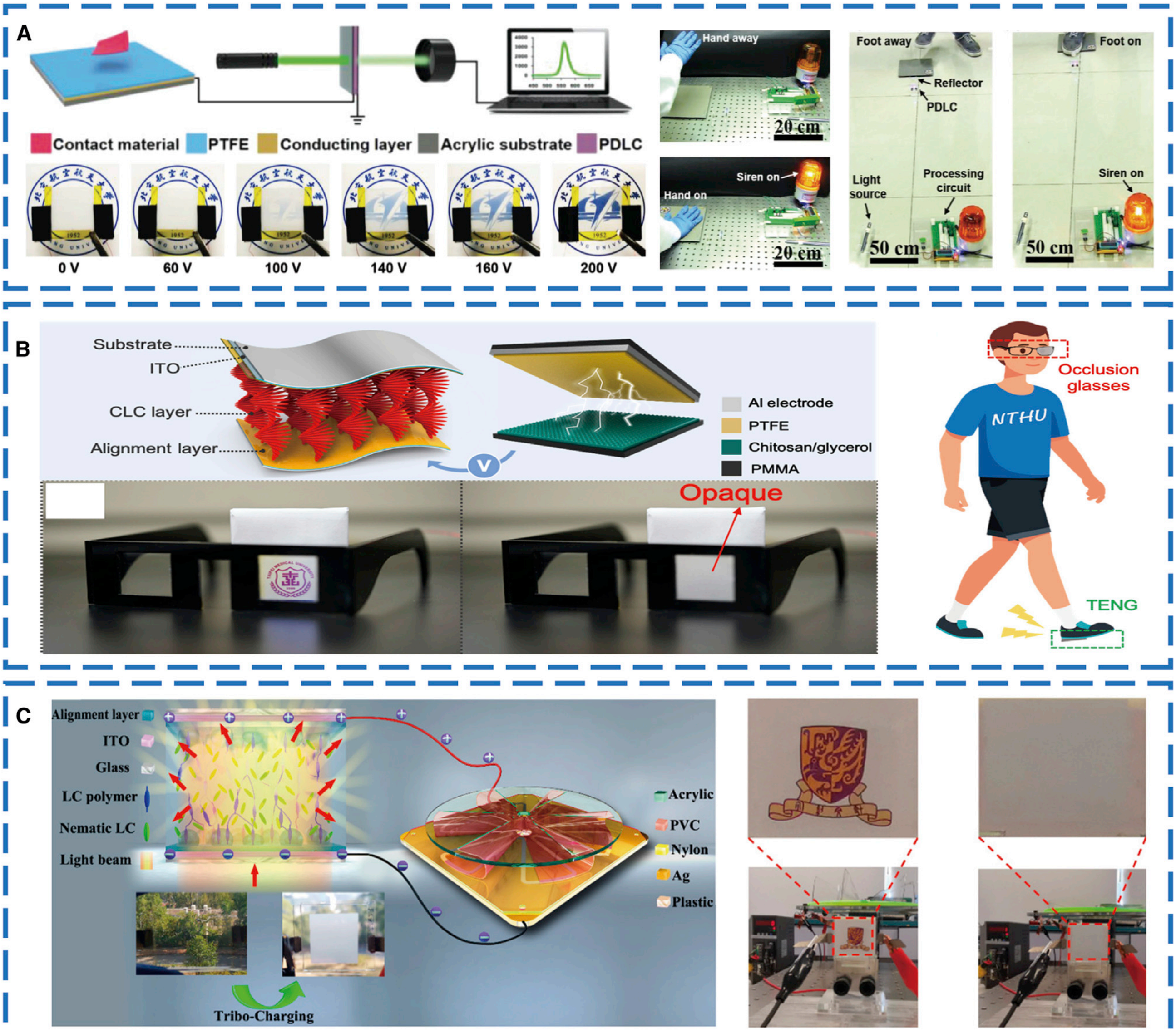

Figure 7. HV-TENGs for liquid crystal modulation

(A) The optical switch for transparency adjustment.[151] Copyright 2019, Wiley-VCH.

(B) The optical switch combined with wearable glasses for amblyopia in children.[152] Copyright 2021, American Chemical Society.

(C) The smart window.[153] Copyright 2020, American Chemical Society.

on a single braille device. This simple, safe, and convenient method is expected to achieve large-scale applications.

Liquid crystal (LC) is a substance with crystal anisotropy and liquid fluidity, showing excellent electro-optic modulation response. Under an appropriate electric field, the arrangement of LC molecules changes, resulting in changes in the propagation path of light. In recent years, LC modulation with TENGs has been studied accordingly. As shown in Figure 7A, Zhang et al. design an optical switch combining a TENG with polymer-dispersed liquid crystal (PDLC).[151] When the 360 V voltage output was applied to the PDLC, the PDLC film rapidly switched from the initial translucent state to an instantaneous transparent state. Moreover, combining the optical switch with signal processing has broad application prospects in monitoring, remote operation, automatic control, and security systems. The cholesteric liquid crystals (CLCs) have bistable properties and can maintain their optical state after removing external stimuli. As shown in Figure 7B, Chen et al. designed an optical switch combining the CS-TENG and CLC.[152] The CS-TENG voltage made the CLCs switch between the three states of planar, focal conic, and homeotropic. The shading rate reached 80% and the device demonstrated high durability up to 500 cycles at 500 V output. Meanwhile, it could be integrated with wearable glasses as an alternative to traditional occlusive therapy for amblyopia in children. The CS-TENG was mounted on the foot to collect the energy from the body's movements and charge the capacitor. Once the switch was closed, the lens changes from transparent to opaque.

Smart windows are on-demand windows that dynamically adjust light transmittance.[154] As shown in Figure 7C, Wang et al. fabricated a self-powered smart window by combining an FR-TENG with polymer network liquid crystal (PNLC).[153] LC polymers and nematic LCs were mixed to form PNLC and encapsulated in aligned layers with randomly distributed microdomains. By applying the more than 1,000 V output from the FR-TENG, the smart window demonstrated an ultra-transparent "OFF" state and an ultra-hazy "ON" state. Its transmittance and haze ratio were as high as 91% and 78%, respectively, and the switching response time of the two states was lower than 7 ms. Based on the above research, they developed a triboelectric smart reflector for self-powered wireless airflow sensing.[155] Due to the dense network structure of the LC polymer, the alignment layer with microdomains, and the small active area, the minimum load charge required for actuation was as low as 7 nC, enabling the monitoring of tiny airflows. The smart windows based on TENG and LC are expected to be used in self-powered skylights, smart agricultural systems, and privacy protection.[156]

The positive and negative charge centers in the unit cell of ferroelectric materials form an electric dipole moment within a certain distance, but the polarization direction is random. By applying electric field, the electric dipole moments direction can become more uniform. When the external electric field reaches a certain value, all the ferroelectric domains have the same polarization direction, which causes the ferroelectric material to reach the saturation polarization state on the macroscopic scale. Based on the controllable spontaneous polarization properties under an applied electric field, combined with TENGs it shows great application potential in the fields of self-powered storage and sensors.[157–159] Fang et al. demonstrated a self-powered ferroelectric transistor memory integrated module based on ferroelectric field effect transistors and a CS-TENG with an output of 220 V.[157] The rectified voltage output of the TENG as the gate voltage was applied to the resistance of the control channel on a flake ferroelectric transistor. The pentacene channel ferroelectric-gate FET exhibited p-type characteristics, and the on/off current ratio was about 10^3. The writing process of ferroelectric transistor memory devices was easily achieved by tapping the TENG with a finger to apply a positive or negative pulse to the gate. The unique bistable ON and OFF current states demonstrated its excellent storage capability.

Application of HV-TENGs for manipulation of fluids and particles

Coulomb forces are ideal driving forces for manipulating macroscopic and microscopic objects. The HV-TENGs combining an electrostatic actuation system (EAS) can have strong control over tiny objects with high precision. They have demonstrated good potential in the fields of microfluidic technology, electroosmosis, electrostatic spraying, and inkjet printing.

Please cite this article in press as: Bai et al., Theory and applications of high-voltage triboelectric nanogenerators, Cell Reports Physical Science (2022), https://doi.org/10.1016/j.xcrp.2022.101108

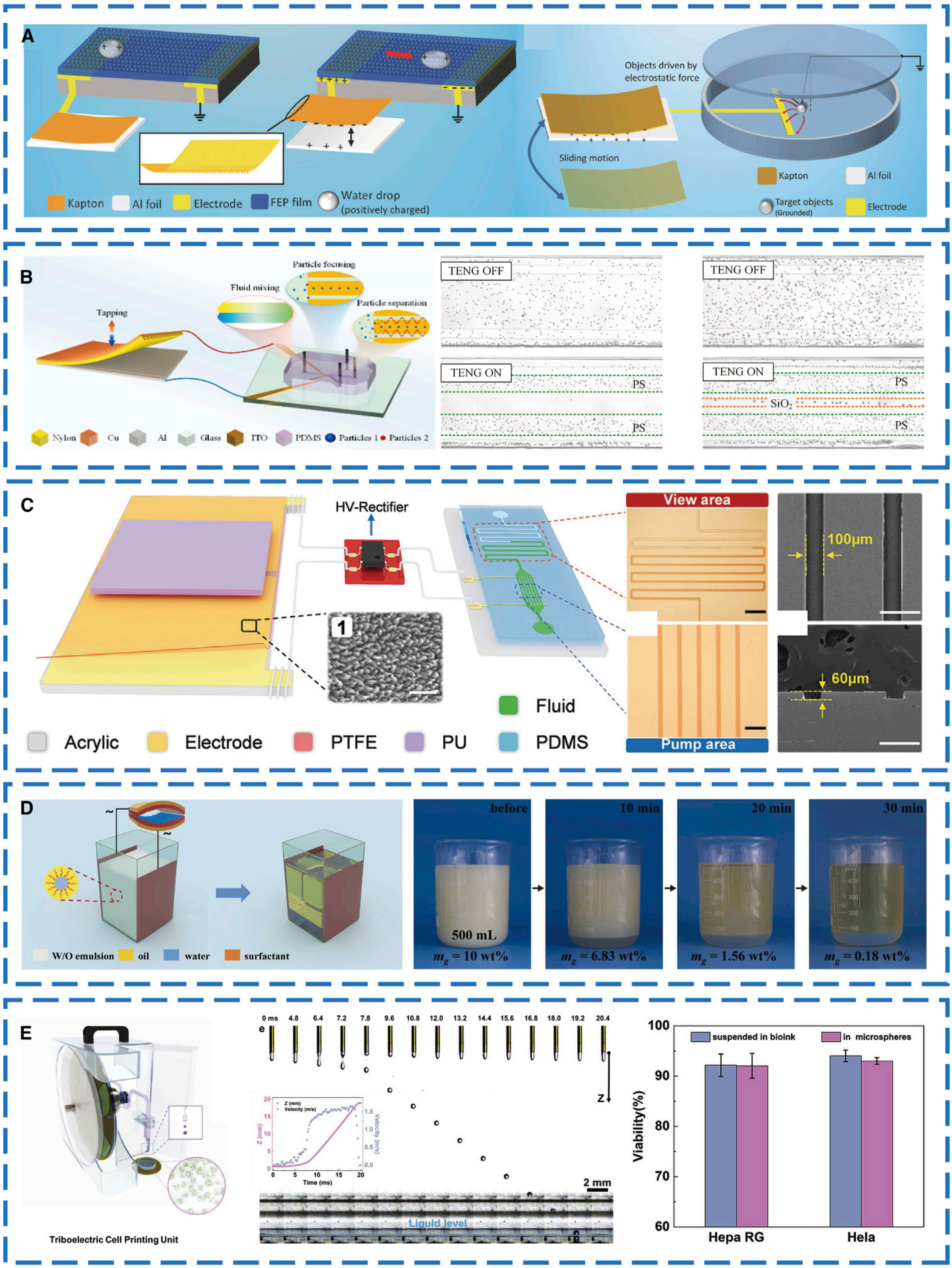

Figure 8. HV-TENGs for the microfluidics motion and tiny solid object control

(A) Self-powered EAS driving micro fluid and small particles.[160] Copyright 2017, Wiley-VCH.

(B) Alternating current electroosmotic flow and induced charge osmotic flow in a microchannel.[162] Copyright 2021, Elsevier.

(C) Triboelectric electroosmotic pump.[121] Copyright 2021, Wiley-VCH.

(D) Water/oil emulsion separation.[96] Copyright 2021, Elsevier.

(E) The electrically assisted cell printing.[115] Copyright 2020, Elsevier.

As shown in Figure 8A, Zheng et al. design two self-powered EASs combining a single-electrode HV-TENG to simultaneously control the microfluidics motion and tiny solid objects.[160] The V_{OC} reached 1.8 kV, which can drive water droplets to move in a 2 cm gap. At the same time, this self-powered current transformer can control the confluence of two droplets with the same charge polarity and different compositions. In addition, based on the same working principle, its ability to manipulate tiny steel balls was demonstrated. In further, Nie et al. fabricated a mini vehicle with four droplets as wheels and combined it with an FS-TENG to carry tiny objects. The V_{OC} of the FS-TENG reached a maximum value of about 3.5 kV. The mini vehicle has a maximum load of 500 mg and a controllable highest velocity is 1 m/s.[125] The droplet moving distance limits its application, which is not only related to the coulomb force, but also to the channel surface morphology. Therefore, they introduced a physical model of self-powered systems based on electrostatic induction theory.[161] Based on an FR-TENG and photo controllable adhesion surface, the output voltage of about 3.4 kV can eject droplets up to 640 mm, achieving a long-distance transport.[112]

Self-powered droplet manipulation systems (SDMSs) demonstrate broad application prospects in the fields of drug delivery, microchemical reactions, and biological microanalysis. As shown in Figure 8B, Zhou et al. combined a TENG with a microfluidic chip to realize alternating current electroosmotic flow (EOF).[162] The longer the unit volume of fluid was exposed to the electric field, the better the mixing effect. Meanwhile, the behavior of particles precise control was also achieved, including the SiO_2 particles assembling under manual operation, and the PS and SiO_2 particle separation. The SDMS designed by Yu et al. can manipulate droplets of multiple compositions to merge and react when the maximum VOC of the FR-TENG reached 5 kV.[124] The SDMS shortened the complete mixing time of droplets of two different components by 6.3 times compared with the passive mixing method.

Electroosmotic pumps are widely used in microfluidic systems due to the advantages of simple fabrication, constant fluid velocity, and high integration. The working principle is to control fluid motion by changing the magnitude and direction of the electric field in the electric double layer (EDL) region. However, an external high-voltage direct current device will form bubbles and generate joule heat near the electrodes, which seriously affects the microfluidics efficiency. Sun et al. reported an efficient triboelectric electroosmotic pump (TEOP).[121] As shown in Figure 8C, the TEOP consists of three parts: an FS-TENG, high-voltage rectifier modules, and microfluidic chips. The FS-TENG generated a VOC of about 35 kV. When the fluid passes through the microchannel, an EDL was formed at the solid-liquid interface. The Stern layer close to the solid-liquid interface had strong electrostatic adsorption, making the ions unable to move. Outside the Stern layer, a diffusion layer formed due to the dynamic balance of positive and negative ions. Applying the external electric field, the net charge ions will drag the liquid molecules to move, forming an EOF. Based on the EOF mechanism, when the FS-TENG slides to the right, a strong leftward electric field will be formed along the EDL channel, driving the EOF to move in the same direction to balance the potential difference. The TEOP reduced the joule heating to only 1.76 J cm^{-3} nL^{-1}. By adjusting the sliding distance, a minimum volume of 0.4 nL can be precisely controlled. This demonstrates the promising application of TEOP in drug delivery and mixing.

In practical applications, various complex motions of droplets need to be manipulated in liquid environments. HV-TENGs can precisely control the various motion behaviors of droplets, which can meet the different application requirements. Wang's team used a HV-TENG to manipulate the water droplet motion in an oil environment, including deformation, reciprocation, adsorption, and ejection.[163] Subsequently, the team applied the above method for water/oil emulsion separation.[96] As shown in Figure 8D, the system consists of a CS-TENG and a set of parallel-plate electrodes. The CS-TENG can generate a V_{OC} of 2,847 V. After 30 min of CS-TENG treatment, the water content in the water/oil emulsion reduced from 5 to 0.15 wt %; the separation efficiency reached 96.97%. This separation method can be applied to oil/water separation, purification, and emulsion separation of industrial lubricating oils.

Electrohydrodynamic jet (e-jet) printing is a high-resolution printed electronics technology that uses an electric field to control droplets. TENG-based e-jet printing systems have attracted the attention of researchers due to their unique advantages, such as portability, safety, and low cost.[164] Huo et al. developed a printing system driven by an FR-TENG for electrically assisted cell printing.[115] As shown in Figure 8E, the printing system consisted of an FR-TENG, a VMC, and a cell printing device. The FR-TENG produced a direct current of up to 5–8 kV. The diameter of microspheres printed by this system was adjustable between 200 and 400 μm, which was suitable for 3D cell culture. In addition, each printed microsphere charge was about 30 pC, proving to be quite safe for cell culture. The printed HepaRG and HeLa cells demonstrated high cell viability (over 92%). This suggests that HV-TENGs can be used as a safe and effective method for electro-assisted cell printing and subsequent biomedical applications.

TENGs have also been applied in electrospinning with the advantages of simple structure, low cost, and high efficiency.[165] Li et al. designed a self-powered electrospinning system composed of an FR-TENG, VMC, and spinneret.[113] The FR-TENG obtained a direct current voltage of 8 kV by a VMC, which can power an electrospinning system for the fabrication of various polymer nanofibers including polyethylene terephthalate (PET), polyamide-6, polyacrylonitrile, PVDF, and thermoplastic polyurethanes. The self-powered electrospinning system designed by Han et al. fabricated Si@void@C nanofibers that can be used as anode materials for lithium batteries, which can realize extremely low-cost electrode material preparation processes.[166]

Based on the fact that static electricity can attract light small objects, electrostatic adsorption technology is produced, which can be used for air purification. A high voltage needs to be applied to the filter. A self-propelled air filtration system based on the combination of HV-TENGs and filter can efficiently remove particulate matters (PMs) in the air. The system has the advantages of low cost, simple device, zero ozone emission, and high filtration efficiency, which can be used for automobile exhaust, industrial exhaust emission treatment, and protective equipment such as masks.

As shown in Figure 9A, Han et al. designed a self-powered triboelectric filter for filtering automobile exhaust PMs.[114] The device consisted of a cuboid chamber with Al electrodes on the upper and lower sides and PTFE pellets placed in the chamber. When the vibration occurs vertically, the PTFE pellets continue to collide with

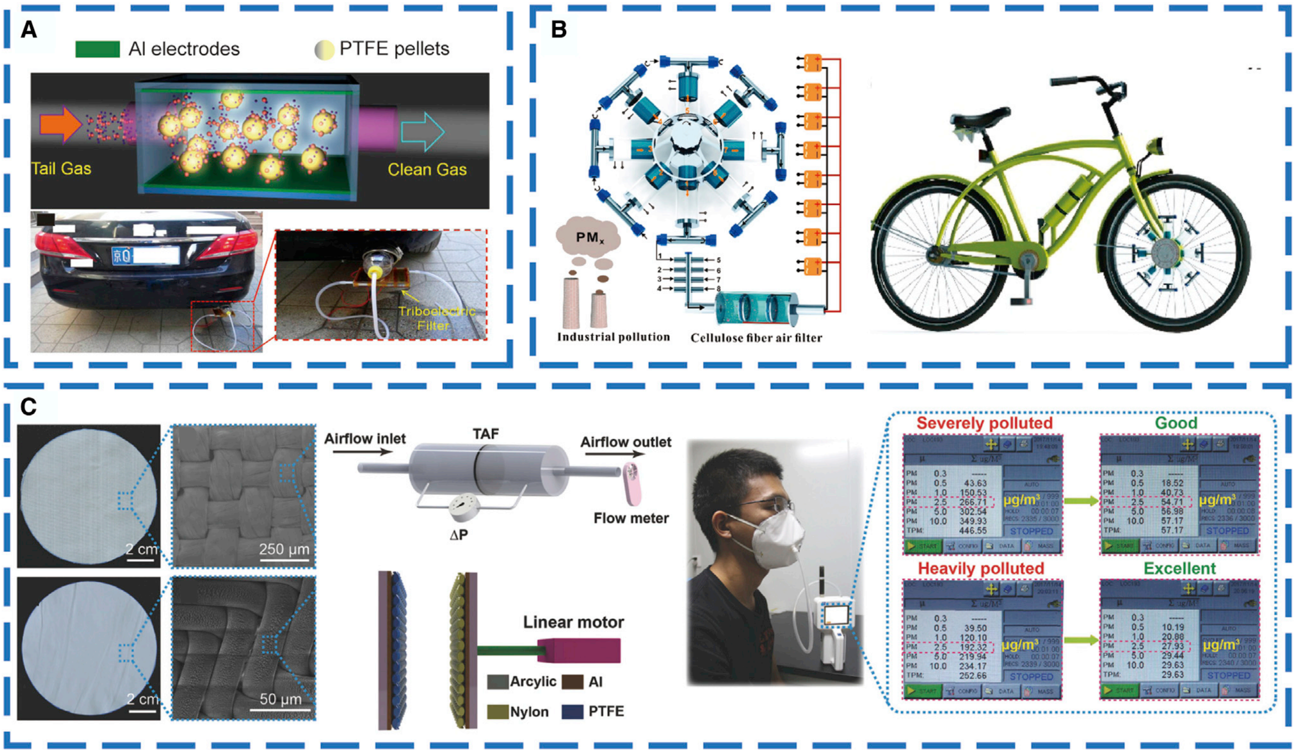

Figure 9. Application of HV-TENG-based adsorption devices

(A) Triboelectric filter for vehicle exhaust treatment.[114] Copyright 2015, American Chemical Society.

(B) A radial piston TENG-enhanced cellulose fiber air filter.[171] Copyright 2020, Elsevier.

(C) A washable triboelectric air filter.[172] Copyright 2018, Wiley-VCH.

the electrodes in the chamber, so that the PTFE pellets are charged with a net negative charge. At the same time, the upper and lower electrodes are also charged with opposite charges, creating a strong electric field in the chamber. When air containing PMs passed through this high electric field area, they are electrostatically attracted and deposited on electrodes or PTFE pellets. The V_{OC} of the device was about 3 kV, which could remove more than 94% of PMs in the aerosol. Even in actual vehicle exhaust treatment, more than ~95.5% of PM2.5 was removed by the vibration of the exhaust tail pipe itself, and the removal efficiency still reached 82.4% after continuous operation of 50 h. Chen et al. fabricated a wind-driven TENG-based air filtration system that not only adsorbed PMs, but also removed SO_2 in the air.[167] Gu et al. designed an rTENG-enhanced PI nanofiber air filter.[168] The PI was made into a nanofiber film on steel mesh by electrospinning. The 90.6% highest removal efficiency was achieved when the PM diameter was 33.4 nm.[169] Feng et al. prepared a self-powered electrostatic filter for degrading formaldehyde by combining photocatalytic technology.[170] The photocatalyst P25 or Pt/P25 was embedded on the surface of polymer-coated stainless steel wire to form a filter network. The V_{OC} of the TENG was over 1 kV, which generated a strong electric field on the filtering network and realized electrostatic and photocatalytic adsorption simultaneously.

In recent years, some new structures of TENG-based air filters have been developed. Yoon et al. designed 3D-printed biomimetic villi structures with a large surface area.[173] Compared with the planar structure, the surface area of the 3D-printed bionic villus structure increased by about 300%, resulting in 5- and 4-fold improvement in power output performance in vertical mode and rotational mode, respectively.

The dust-adsorption system based on this structure effectively absorbed dust particles of various sizes. Mo et al. designed a radial piston TENG-enhanced cellulose fiber air filter.[171] As shown in Figure 9B, the eight piston-type TENG units were evenly distributed on the same horizontal plane in a 45° radial arrangement. Connecting two one-way valves to each TENG unit effectively controlled the airflow into the air filter. When the rotor rotated 360°, each piston TENG completed one motion cycle. The removal efficiencies of PM2.5 and PM10 by this piston-type TENG-based air filter were 83.78% and 86.82%, respectively. The system can collect rotational mechanical energy from a bicycle movement for instantly remove PMx from the surrounding air, realizing a truly self-powered air filter system.

In addition to self-powered air filter systems, TENGs have also been widely applied as wearable air filter devices for human protection. Liu et al. designed a self-powered mask based on a breath-driven TENG and PVDF electrospinning nanofiber film.[174] During respiration, the self-powered mask can remove coarse and fine particles with an efficiency of higher than 99.2 wt %. Cheng et al. developed a smart mask based on polyetherimide (PEI) electrets that can both remove particles and monitor respiration.[175] He et al. proposed a cellulose fiber TENG filter with a silver nanofiber film, which showed good antibacterial activity.[176] Ghatak et al. designed a face mask consisting of a triboelectric filter and an electrocution layer for filtering and inactivating SARS-CoV-2. The electric field caused viral exterior protein inactivation and virus death.[177] To enable sustained adsorption capacity and long usage of self-powered wearable air filter devices, Bai designed a washable triboelectric air filter that can be used multiple times.[172] As shown in Figure 9C, it is composed of five layers of PTFE fabric and nylon fabric. The output of constructed CS-TENG reached 190 V. Considering its usage as a wearable mask, the voltage is relatively high. The contact between PTFE and nylon was charged to adsorb small particles, and the removal efficiency for PM0.5 and PM2.5 increased from 26.3% to 84.7%, and 69.1% to 96.0% after the fabrics were rubbed with sufficient charges. The removal efficiency remained almost unchanged after multiple washings. Wang et al. designed a polyvinyl alcohol (PVA) medical mask.[178] The PVA rich in hydroxyl groups can spontaneously form hydrogen bonds with water vapor molecules exhaled by the human body, fixing the role of water molecules, which solves the problem of excessively fast charge dissipation in the middle adsorption layer of traditional PP-based medical masks during long-term use.

HV-TENGs for ionization

In a high-voltage electric field, gaseous substances are ionized into positive and negative ions, forming plasma (neutral ionized gaseous substances), which is regarded as the fourth state of matter. Plasma plays an important role in the fields of biomedicine, semiconductors, nanotechnology, and surface treatment. Plasma excitation requires a high-voltage source, but conventional high-voltage sources suffer from the disadvantages of high cost, limited portability, and safety issues. HV-TENGs have the advantages of simple structure and low cost. Moreover, they are highly safe devices because the current is only microampere level. Therefore, HV-TENGs are excellent candidates for plasma excitation. Cheng et al. successfully excited four typical atmospheric pressure plasmas (dielectric barrier discharge [DBD], atmospheric pressure non-equilibrium plasma jet, corona discharge, and spark discharge) using an FR-TENG, as shown in Figure 10A.[179] The V_{OC} of the FR-TENG exceeded 1 kV under 463 rpm. When argon gas was passed through the capillary, a distinct microplasma plume was observed. The effects of different parameters, including electrode spacing, electrode diameter, and gas flow rate, on the performance of the microplasma were analyzed. Later, taking the DBD

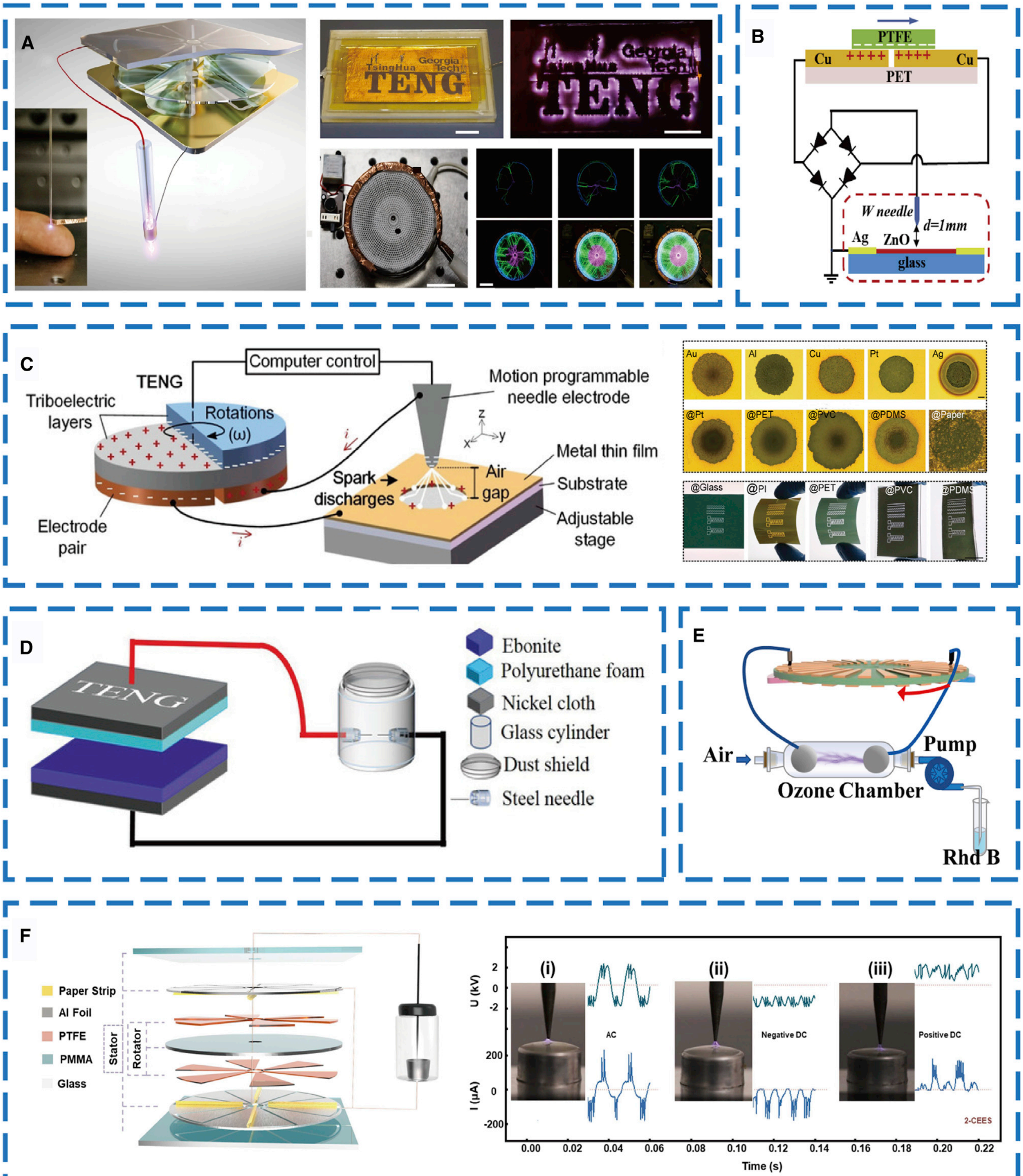

Figure 10. HV-TENGs enable a variety of applications related to ionization

(A) Microplasma excitation using an FR-TENG.[179] Copyright 2018, Springer Nature.

(B) Microplasma modulating the Schottky barrier height of Ag/ZnO nanowires.[181] Copyright 2019, Elsevier.

Figure 10. *Continued*

(C) Spark discharge for metal micropattern fabrication.[182] Copyright 2021, Wiley-VCH.
(D) A self-powered ammonia synthesis system.[91] Copyright 2019, Wiley-VCH.
(E) An ozone generator for water treatment.[103] Copyright 2021, Elsevier.
(F) Chemical warfare agent decontamination based on microplasma and ozone generation.[105] Copyright 2022, Elsevier.

microplasma as an example, they utilized a capacitive-impedance loading method to improve the high-voltage field output performance of FR-TENG.[180] By increasing the input frequency or reducing the gas pressure, the discharge intensity and efficiency were improved, and the discharge power was increased more than 10 times.

Charged ions and functional groups can be adsorbed on the surface of 1D or 2D materials, making it a good strategy for tuning the performance of functional devices. Cheng's team developed a surface ion gate modulation technique based on an FS-TENG-driven microplasma that can effectively modulate the Shottky barrier height and electrical transport properties of Ag/ZnO nanowires.[181] As shown in Figure 10B, the Ag/ZnO nanowire surface was treated by microplasma excited via the FS-TENG after rectification. The VOC of the FS-TENG reached 1,320 V. Due to the negative corona discharge, a large number of oxygen anions were generated around the anode and adsorbed on the ZnO nanowire surface. This made the ZnO fermi level decrease to a level lower than the surface state energy level, increasing the height of the Schottky barrier. Combining ion gate modulation with ultraviolet (UV) irradiation enables reversible modulation of the barrier height. The ion gate modulation shortened the recovery time of ZnO nanowire UV light detection from 87 to 0.3 s. Later, the tuning of the carrier concentration of the 2D monolayer MoS_2[117] and the surface ions of $Cd(OH)_2$@ZnO nanowires were also realized by this technique.[183]

The instantaneous temperature of local spark discharge can reach 10,000°C, which is often used to cut metal in the mechanical manufacturing field. Wang et al. proposed a triboelectric spark discharge method to fabricate metal micropatterns.[182] As shown in Figure 10C, the triboelectric spark discharge micropattern system consisted of an FR-TENG and a motion programmable needle electrode. The FR-TENG generated an alternating high electric field between the needle electrode and the metal thin film, generating spark discharges in the air gap. During the discharge process, electrical energy was converted into heat energy, which etches metal materials through high temperature melting and evaporation. Films (100 nm thick) of different metals, including Au, Al, Cu, Pt, and Ag, pre-deposited on glass substrates were processed with this device, and all showed obvious etching effect. PI, PET, PVC, PDMS, and paper have all been used as substrates to etch metal thin films by triboelectric spark discharge without causing significant damage to the substrates. Moreover, the triboelectric spark discharge can also process carbon-based materials and conductive polymers, demonstrating great potential in the manufacture of flexible electronic devices.

Air is a rich nitrogen source. Nitrogen fixation is the conversion of nitrogen in the air into nitrogen compounds. HV-TENG-driven discharge is a feasible and ideal strategy to nitrogen fixation. Wong et al. designed a TENG-driven nitrogen fixation system (Figure 10D).[91] The CS-TENG can outputted about 1,300 V without any auxiliary, which can convert nitrogen gas into nitrogen dioxide by microplasma discharge and eventually nitrate in an aqueous solution. A NO_3^- concentration of 250 ppm can be arrived after 400 min. Han et al. designed a self-powered electrocatalytic ammonia synthesis system based on a dual-FR-TENG device and ammonia synthesis devices.[106] By introducing the dual-TENG structure, nitrogen fixation and electrocatalytic reduction were performed simultaneously. A 10-stage VMC was connected to

TENG-1 to obtain V_{OC} of about 7 kV. When TENG-1 worked, a strong electric field was generated to ionize nitrogen and oxygen molecules between the needle-plate electrodes to form NO_x. The NO_x-containing gas stream entered the water-scrubbing cylinder through the pipeline to form the electrolyte of NO_3^- and NO_2^-, TENG-2 drives the subsequent electrocatalytic reduction of ammonia synthesis. Under the simulated exhaust gas flow rate of 3.5 m^3 min^{-1}, the self-powered electrocatalytic system produced 2.4 $\mu g\ h^{-1}$ of ammonia at ambient conditions. Later, driven by simulated exhaust gas, a Tesla turbine TENG was designed for nitrogen fixation under corona discharge, and the ammonia synthesis system achieved a yield of 2.14 $\mu g\ h^{-1}$ under ambient conditions.[107] Compared with traditional synthesis methods, the TENG-driven nitrogen fixation system is environmentally friendly and endowed with other merits, including self-powering, low cost, and convenient fabrication, demonstrating great potential in the field of ammonia synthesis.

In addition to nitrogen ions, ozone can also be generated in corona discharge in the air. As shown in Figure 10E, Lei et al. designed a multifunctional water purification system with self-powered ozone generation based on a ''like charges repel'' TENG (LCR-TENG) and a corona discharge chamber.[103] The maximum voltage of the LCR-TENG exceeded 30.7 kV, and the maximum concentration of ozone generated reached 30 mg/m^3. Subsequently, Luo and Chen and co-workers fabricated a self-powered UV sterilizer system for water sterilization based on high-voltage TENG and UV lamps.[102,184] The self-powered ozone generator was combined with UV sterilization to effectively kill bacteria in the water, providing a new idea for a hybrid purification system. Ozone, a strong oxidant, can oxidize organic matters into respective oxides, as is used for pollutant treatment. Bai et al. proposed a self-powered chemical warfare agent degradation system based on a double-layer paper-strip rotary TENG (dps-rTENG), as shown in Figure 10F.[105] The dps-rTENG generated a V_{OC} of about 3 kV. Microplasma and ozone were successfully generated under the alternating current, positive direct current, and negative direct current modes, respectively. The degradation efficiency of 2-chloroethylethyl sulfide reached more than 99% within 2 min; and the energy utilization efficiency of the dps-rTENG was 0.520 μg/J, one order of magnitude higher than commercial power supplies. Triboelectric microplasma and ozone generation provides a new avenue for future self-powered, portable disinfection systems.

Substance ionization exhibits potential applications in species detection/synthesis. Li et al. proposed a nano-coulomb ionization system for mass spectrometry using the HV-TENGs to generate alternating polarity ion pulses.[185] The high voltage ensured the ionization of the molecular, and the low-current quantitatively controlled the total ionization charges in mass spectrometry. The two features improved sample utilization and enabled high sensitivity of substance detection. The detection limit reached as low as 10 pg mL^{-1} for cocaine. TENG-mass spectrometry successfully analyzed a wide variety of compounds, including small organic molecules and biological macromolecules. Bernier et al. also used this method to identify the components of multiple falsified antimalarial drugs.[186]

Application of HV-TENGs in biological fields

When a strong external electric field is applied to the cells, it causes the cell membrane permeability to change by forming nanoscale pores, which is called electroporation, and can be used for gene therapy, drug delivery, and sterilization. Generating strong electric fields requires a high-voltage source. Typically, commercial electroporation equipment is bulky and expensive. On the contrary, TENGs can generate high voltage with simple structure, low cost, and light weight. Luo et al. designed a self-powered water sterilization device composed of an FR-TENG, a VMC, and a water droplet control system.[104] Aided by the VMC, the FR-TENG generated a high voltage of 9,319 V, and the electric field strength reached 11.28 kV cm^{-1}, resulting in quick death of both Gram-negative *Escherichia coli* and Gram-positive *Staphylococcus aureus*. Cho et al. designed a sterilization system based on the TENG electroporation and filtration effects of conductive cellulose film. It achieved 100% microbial removal efficiency after three filtration cycles.[187] In addition to water disinfection, Chiu et al. fabricated a human-driven self-powered disinfection system with multilayer TENG and conductive fabric electrodes that can be placed on the sole.[188] The working principle of this system was based on the mixed effect of electroporation and H_2O_2 production, demonstrating a good disinfection performance against *E. coli* and *S. aureus*.

Apart from applying very high voltage to plain electrodes, strong electric fields can also be generated by applying less high voltage to micro-nano electrodes. As shown in Figure 11A, micro-nano electrodes, which have very small tip sizes, can generate enhanced electric field near their tips. Here, HV-TENGs with low-current output have an in-depth advantage in that they can avoid impairing the subtle micro-nano electrodes, as well as the cells and organs. Recently, HV-TENG-based micro-nano electrode-assisted electroporation have been successfully applied to do sterilization and cellular substance delivery.

Tian et al. designed a self-powered highly efficient water disinfection system.[192] It consisted of a ball-shaped TENG and ZnO nanowire electrodes loaded with silver nanoparticles. Based on the synergistic effect of the local electric field enhanced by electroporation of ZnO nanowires and reactive oxygen species generated by Ag nanoparticles, the colony forming units of Gram-negative bacteria decreased from 10^6/mL to 0 within 0.5 min. In addition, the ability to destroy bacteria was maintained for at least 20 min after the electric field was not applied, which can be effectively used for timely and sustainable water sterilization, respectively. Huo et al. fabricated a TENG-driven and CuP_3 nanowire enhanced rapid disinfection system.[189] As shown in Figure 11A, it mainly consisted of a CS-TENG and a three-electrode disinfection filter. Here, the three-electrode disinfection filter consisted of a four-layer stainless steel mesh as the negative electrode, a copper phosphide nanowire modified copper plate electrode as the positive electrode, and a stainless-steel ground electrode placed in the pipeline. When air flowed through the pipeline, the bacteria and viruses in the air first passed through the stainless-steel mesh electrode and became negatively charged. Next, charged microorganisms flowed between the positive and ground electrodes. Due to the short distance between the positive electrode and the ground electrode, a strong electric field was generated between the positive electrode and the ground electrode. When the negatively charged microorganisms flowed through, the microorganisms were immediately trapped on the surface of the Cu3PNW modified positive electrode by electrostatic attraction. A localized electric field of more than 107 V/m was generated near the nanowire tip driven by the CS-TENG. More than 99.99% of bacteria and viruses were inactivated at 2 m/s gas velocity. The device exhibits great potential in rapid indoor air disinfection systems, even water sterilization.

TENG-based electroporation technology has also been successfully applied for cell manipulations. As shown in Figure 11C, Zhao et al. designed a self-powered drug release system based on a magnetic TENG (MTENG)-induced electroporation of red blood cells (RBCs) for tumor therapy.[190] With the aid of microneedle electrodes, the local electric field reached about 4 kV/cm. The electric field generated

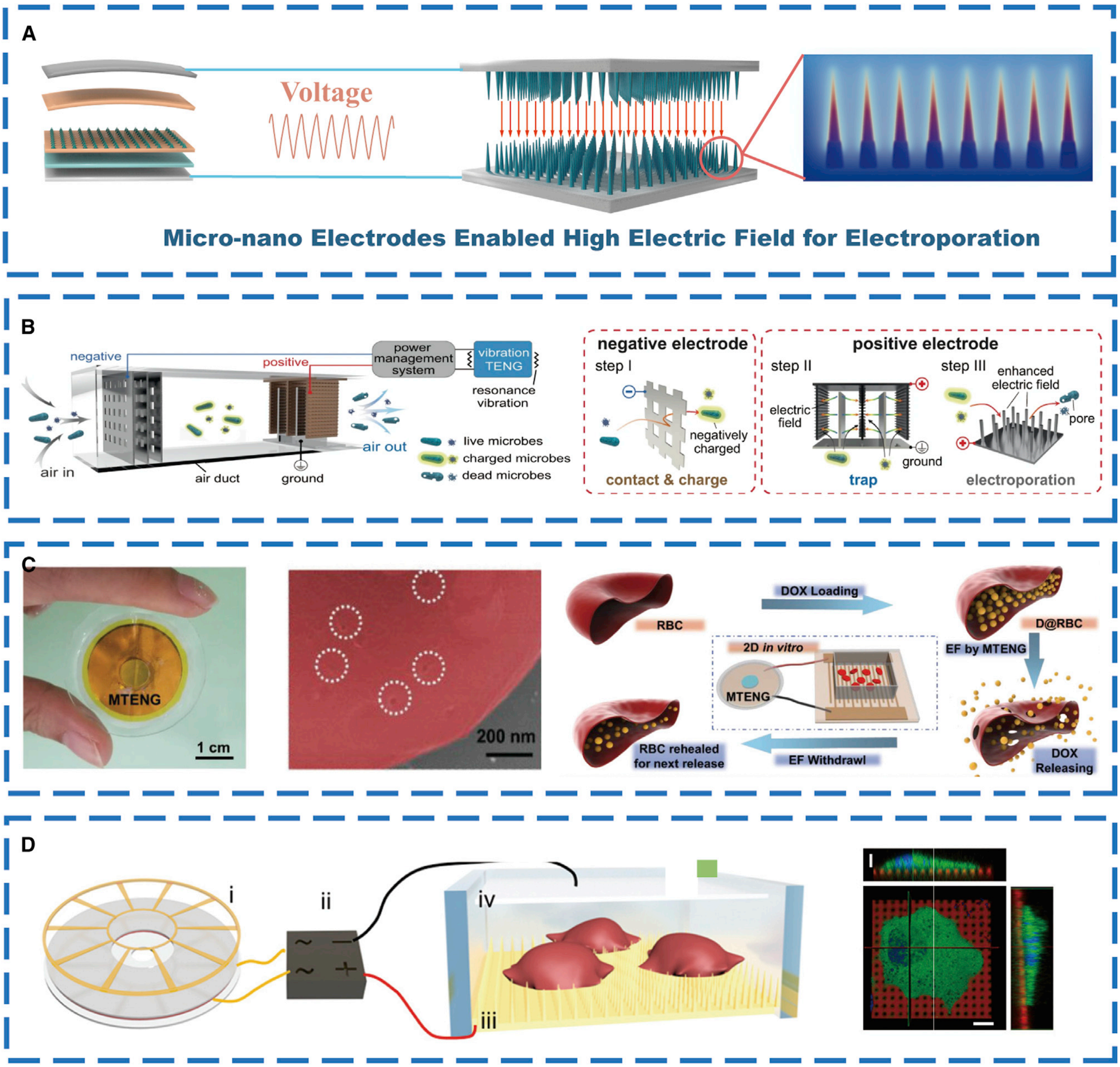

Figure 11. TENG-based electroporation systems

(A) Micro-nano electrodes enabling high electric field for electroporation.

(B) TENG-based electroporation system for air sterilization.[189] Copyright 2021, Springer Nature.

(C) MTENG-based RBC electroporation system with controlled drug release for anti-tumor therapy.[190] Copyright 2021, Wiley-VCH.

(D) The self-powered cell electroporation system for drug delivery.[191] Copyright 2019, Wiley-VCH.

nanopores on the RBCs, which were the drug vehicle. The release of doxorubicin loaded in the RBCs increased and decreased simultaneously upon the application and withdrawal of the electric field, greatly improving the anti-tumor efficiency. Due to the advantages of TENG high voltage and low current, electroporation only acts on tiny-sized RBCs, avoiding harmful effects of high current stimulation on cells and tissues. Later, Yang et al. developed a TENG-driven nanowire electrode array to facilitate siRNA delivery into cells.[193] All six cell lines transfected achieved high cell viability. Liu et al. designed a high-throughput self-powered electroporation system based on TENG and polypyrrole microfoam electrodes modified with silver nanowires.[194] The self-powered electroporation system delivered different sized biomolecules into different cell lines with an efficiency of up to 86% and cell viability of over 88%. Based on the above work, they demonstrated an in-depth application of drug delivery in mice.[191] As shown in Figure 11D, the device consisted of an FR-TENG and silicon nanoneedle array electrodes. In cell experiments, efficient delivery of exogenous substances was demonstrated. In particular, the material delivery of difficult-to-transfer primary cells showed a delivery efficiency of up to 90% and a cell viability of over 94%. In mice experiments, TENG electroporation was demonstrated for dextran-FITC drug delivery *in vivo*. The drug delivery amount of the TENG-driven and nanoneedle-assisted electroporation far exceeded that of the nanoneedles alone by more than 3-fold. These results demonstrated the feasibility of using TENGs for *in vivo* drug delivery.

In addition to the biological applications of electroporation and drug delivery, HV-TENGs can also contribute to agricultural production. In agricultural production, an external high electrostatic field can accelerate seed germination and plant growth. Li et al. reported an all-weather TENG (AW-TENG) for plant seed germination.[100] The AW-TENG was an integration of a bearing-and-hair TENG (BH-TENG) and a raindrop-driven TENG (R-TENG), which can harvest wind and rain energy, respectively. The V_{OC} of the BH-TENG was over 3 kV under simulated natural wind, and the instantaneous output power density of R-TENG reached about 1 W m^{-2}. Under the electric field treatment, the germination rate of pea seeds was increased by about 26.3% and the yield increased by about 17.9%. The mechanism was that the electric field promoted the photosynthesis of seedling growth, improved the nitrogen absorption and transformation efficiency, and alleviated the peroxidation of the inner cells. The combination of BH-TENG with R-TENG also realized driving thermos-hygrometers for agricultural sensing. Moreover, Hu's team designed a polyester fur-enhanced ternary dielectric rotary TENG (PFR-TENG) with low friction loss, and the PFR-TENG could maintain 100% electrical output after 100k cycles.[99] By adopting ternary dielectric design, the DC voltage reached 15 kV and AC voltage reached 10 kV without a voltage multiplying circuit. The electric field generated by PFR-TENG was used to promote tomato seed germination. The germination index and vigor index increased by 34.4% and 351.2%, respectively (Figure 12). These HV-TENG-based agricultural systems provide a new technical solution for the development of intelligent agriculture.

SUMMARY AND PROSPECTS

As emerging energy-harvesting devices, TENGs have demonstrated inherent characteristics of high voltage and low current, and attracted attention from many researchers. This paper systematically reviews the theories, the fabrication, and the applications of the HV-TENGs, those with outputs up to thousands of volts. By summarizing the theories of the TENG voltage generations of the four models, we come to a conclusion that the output is mainly affected by the surface charge density. However, to generate thousands of volts, common approaches to enhance surface charge density are no longer applicable. Therefore, unique strategies to elevate the output voltage of TENGs are introduced, including reasonable structural designs, and special energy management. Various charge supplementary, charge pumping, and charge storage structures have been invented to fulfill the high surface charge requirement of HV-TENGs. Meanwhile, VMCs consisting of series of diodes and capacitors have demonstrated the capability to elevate the output severalfold.

Please cite this article in press as: Bai et al., Theory and applications of high-voltage triboelectric nanogenerators, Cell Reports Physical Science (2022), https://doi.org/10.1016/j.xcrp.2022.101108

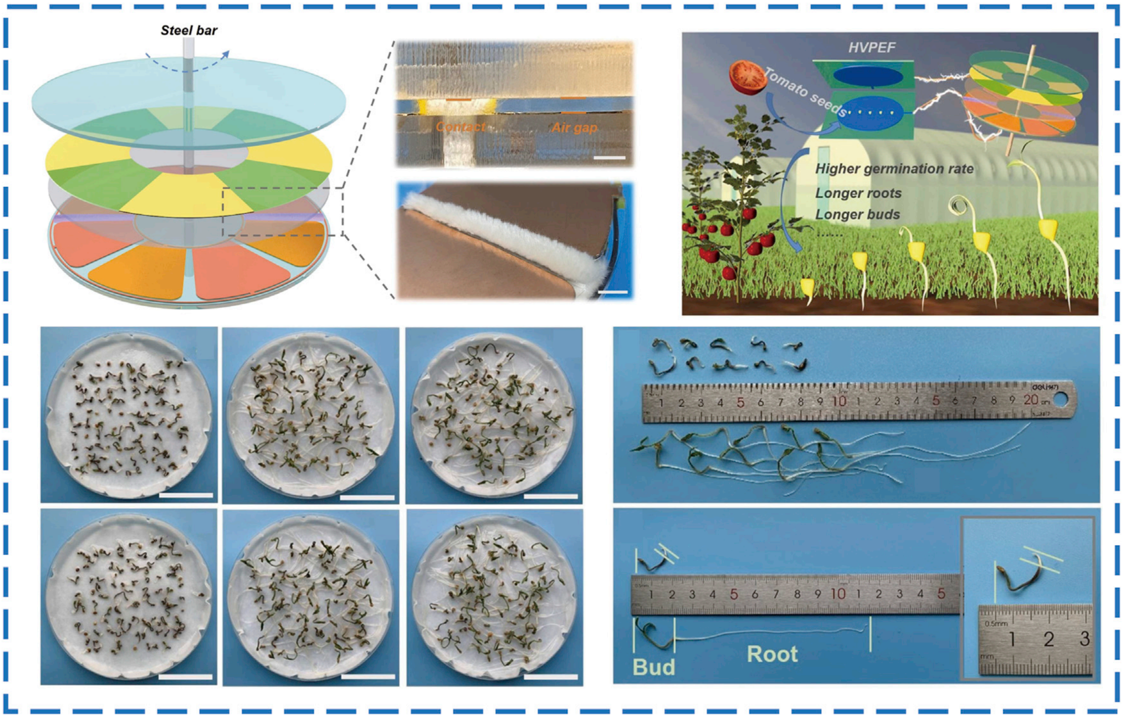

Figure 12. The HV-TENG-based smart agricultural system
Reproduced with permission from Li et al.[99] Copyright 2021, Elsevier.

After successful fabrication of the HV-TENGs, many featured applications have been derived. For example, under a high voltage, the dielectric elastomer deforms, which promotes the development of grating adjustment, self-driving robots, and braille-recognition systems. In the same way, HV-TENGs modulate LC materials and ferroelectric materials and enable their applications in smart windows and transistor memory modules. In a micro-view, charged small particles, including electrons or ions, move under the action of electrostatic forces. In some conditions, ionization is directly achieved by the high voltage of the HV-TENGs. Based on these facts, a series of HV-TENG-based systems for microfluidic control, self-driven printing, air purification, and plasma excitation, are introduced. In addition, biological tissues and cells also have special responses toward HV-TENGs, including reversible electroporation for gene or drug delivery, and irreversible electroporation for sterilization. In addition, the application of HV-TENGs in plant growth and environmental monitoring may largely promote the development of smart agriculture.

The designs and applications of HV-TENGs have demonstrated their special working principles and unique advantages. These include economical materials, easy fabrication, small size, high safety, and high energy efficiency. Among them, high safety is the most irreplaceable merit, which is due to their large inherent resistance. HV-TENGs give voltages of several kV accompanied with currents of several μA, making them safe for biomedical applications. For instance, HV-TENGs have distinguished high electric field from high voltage, which were used without distinction for existing commercial power supplies. Due to the low-current output characteristics, TENGs can avoid impairing the subtle micro-nano electrodes even at thousands of volts. This in turn greatly encourages combinations with TENGs and micro-nano electrodes to generate high electric field at lower voltage. This has enabled selective and reversible electroporation of micro-organisms and cells, and more applications can be expected.

The following are some directions for the future development of HV-TNEGs.

1. To further solve the problem of instability of TENGs. In practical applications of TENGs, a long-term operation is required, which presents a challenge to the stability of TENGs. This needs to be solved in the form of material and structural design. In terms of materials, it is necessary to develop materials with wear-resistance to reduce friction loss between materials. It is also needed to limit the dissipation of surface charges, such as preventing the drift of charges between the triboelectric and the electrode layer, and the breakdown between the friction layers. Reasonable structural design, including flexible contact and lubrication, can greatly extend the working life of the HV-TENGs.
2. To make better use of the environmental mechanical energy. TENGs are self-powered in that they can convert mechanical energy into electricity. However, environmental mechanical motion is often irregular; for example, ocean energy possesses a random direction and inhomogeneous energy pattern. Right now, many HV-TENGs require a stable power supply. Therefore, the future HV-TENGs designs should take into consideration the irregular movement energy collection, such as those developed for ocean energy collection: the nodding duck structure,[195] the seesaw structure,[196] and the honeycomb-like structure.[197] Meanwhile, it is very helpful to develop energy management modules (rectifiers, or filter circuits) and matchable energy storage modules (batteries or capacitors) to store the converted electricity and then make a stable output.
3. To extend the applications in the biomedical fields. Based on the diversified structural designs of HV-TENGs, they can be applied to various application scenarios. Many devices with unique functions coupled with TENGs are yet to be developed, especially in the biomedical fields. The high-voltage and low-current characteristics may be very helpful for cancer therapy: to induce tumor ablation with less heat, less pain, and no harm to the cardiovascular system. In addition, HV-TENGs are very promising in drug delivery and electrical stimulation for muscles. The interactions of high voltage with the skin (high resistance) and the muscles and organs (low resistance) are worth further exploration.

ACKNOWLEDGMENTS

This work is supported by the National Key R&D Program of China (2021YFB3200600), the Fundamental Research Funds for the Central Universities, the National Natural Science Foundation of China (81971770, T2125003, and 61875015), Beijing Natural Science Foundation (JQ20038), and the Strategic Priority Research Program of the Chinese Academy of Sciences (XDA16021101).

AUTHOR CONTRIBUTIONS

Y.B., H.F., and Z.L. proposed the topic of the review. Y.B. wrote the manuscript. H.F. and Z.L. performed the literature review and summary. H.F. and Z.L. revised a draft of the review.

DECLARATION OF INTERESTS

The authors declare no competing interests.

REFERENCES

1. Carneiro, P.M., Vidal, J.V., Rolo, P., Peres, I., Ferreira, J.A., Kholkin, A.L., and Soares dos Santos, M.P. (2022). Instrumented electromagnetic generator: optimized performance by automatic self-adaptation of the generator structure. Mech. Syst. Signal Process. *171*, 108898.

2. Xu, Y., Zhang, Z., Bian, Z., and Yu, L. (2020). Dynamic performance improvement of doubly salient brushless DC generator system with controlled rectifier. IEEE Trans. Ind. Electron. *67*, 8209–8218.

3. Kim, H.-S., An, Y.-J., Kwak, J.I., Kim, H.J., Jung, H.S., and Park, N.-G. (2022). Sustainable green process for environmentally viable perovskite solar cells. ACS Energy Lett. *7*, 1154–1177.

4. Li, M., Feng, S., Shen, S., Huang, H., Xue, W., Yu, N., Zhou, Y., Ma, W., Song, J., Tang, Z., and Bo, Z. (2022). High efficiency ternary organic solar cells via morphology regulation with asymmetric nonfused ring electron acceptor. Chem. Eng. J. *438*, 135384.

5. Zhan, L., Li, S., Li, Y., Sun, R., Min, J., Bi, Z., Ma, W., Chen, Z., Zhou, G., Zhu, H., et al. (2022). Desired open-circuit voltage increase enables efficiencies approaching 19% in symmetric-asymmetric molecule ternary organic photovoltaics. Joule *6*, 662–675.

6. Mao, J., Liu, Z., Zhou, J., Zhu, H., Zhang, Q., Chen, G., and Ren, Z. (2018). Advances in thermoelectrics. Adv. Phys. X. *67*, 69–147.

7. Lindorf, M., Mazzio, K.A., Pflaum, J., Nielsch, K., Brütting, W., and Albrecht, M. (2020). Organic-based thermoelectrics. J. Mater. Chem. A Mater. *8*, 7495–7507.

8. Falconi, C. (2019). Piezoelectric nanotransducers. Nano Energy *59*, 730–744.

9. Wang, Z.L., and Song, J. (2006). Piezoelectric nanogenerators based on zinc oxide nanowire arrays. Science *312*, 242–246.

10. Xu, Q., Wen, J., and Qin, Y. (2021). Development and outlook of high output piezoelectric nanogenerators. Nano Energy *86*, 106080.

11. Zhong, W., Xu, L., Zhan, F., Wang, H., Wang, F., and Wang, Z.L. (2020). Dripping channel based liquid triboelectric nanogenerators for energy harvesting and sensing. ACS Nano *14*, 10510–10517.

12. Fan, F.-R., Tian, Z.-Q., and Lin Wang, Z. (2012). Flexible triboelectric generator. Nano Energy *1*, 328–334.

13. Gai, Y., Bai, Y., Cao, Y., Wang, E., Xue, J., Qu, X., Liu, Z., Luo, D., and Li, Z. (2022). A gyroscope nanogenerator with frequency up-conversion effect for fitness and energy harvesting. Small *18*, 2108091.

14. Gu, L., German, L., Li, T., Li, J., Shao, Y., Long, Y., Wang, J., and Wang, X. (2021). Energy harvesting floor from commercial cellulosic materials for a self-powered wireless transmission sensor system. ACS Appl. Mater. Interfaces *13*, 5133–5141.

15. Zhang, N., Qin, C., Feng, T., Li, J., Yang, Z., Sun, X., Liang, E., Mao, Y., and Wang, X. (2020). Non-contact cylindrical rotating triboelectric nanogenerator for harvesting kinetic energy from hydraulics. Nano Res. *13*, 1903–1907.

16. Ko, H.-J., Kwon, D.-S., Bae, K., and Kim, J. (2022). Self-suspended shell-based triboelectric nanogenerator for omnidirectional wind-energy harvesting. Nano Energy *96*, 107062.

17. Zhang, L., Meng, B., Tian, Y., Meng, X., Lin, X., He, Y., Xing, C., Dai, H., and Wang, L. (2022). Vortex-induced vibration triboelectric nanogenerator for low speed wind energy harvesting. Nano Energy *95*, 107029.

18. Wang, Y., Yang, E., Chen, T., Wang, J., Hu, Z., Mi, J., Pan, X., and Xu, M. (2020). A novel humidity resisting and wind direction adapting flag-type triboelectric nanogenerator for wind energy harvesting and speed sensing. Nano Energy *78*, 105279.

19. Xu, Y., Yang, W., Lu, X., Yang, Y., Li, J., Wen, J., Cheng, T., and Wang, Z.L. (2021). Triboelectric nanogenerator for ocean wave graded energy harvesting and condition monitoring. ACS Nano *15*, 16368–16375.

20. Zhang, C., Zhou, L., Cheng, P., Liu, D., Zhang, C., Li, X., Li, S., Wang, J., and Wang, Z.L. (2021). Bifilar-pendulum-assisted multilayer-structured triboelectric nanogenerators for wave energy harvesting. Adv. Energy Mater. *11*, 2003616.

21. Jiang, T., Pang, H., An, J., Lu, P., Feng, Y., Liang, X., Zhong, W., and Wang, Z.L. (2020). Robust swing-structured triboelectric nanogenerator for efficient blue energy harvesting. Adv. Energy Mater. *10*, 2000064.

22. Fan, K., Wei, D., Zhang, Y., Wang, P., Tao, K., and Yang, R. (2021). A whirligig-inspired intermittent-contact triboelectric nanogenerator for efficient low-frequency vibration energy harvesting. Nano Energy *90*, 106576.

23. Wu, C., Liu, R., Wang, J., Zi, Y., Lin, L., and Wang, Z.L. (2017). A spring-based resonance coupling for hugely enhancing the performance of triboelectric nanogenerators for harvesting low-frequency vibration energy. Nano Energy *32*, 287–293.

24. Xu, W., Zheng, H., Liu, Y., Zhou, X., Zhang, C., Song, Y., Deng, X., Leung, M., Yang, Z., Xu, R.X., et al. (2020). A droplet-based electricity generator with high instantaneous power density. Nature *578*, 392–396.

25. Chen, Y., Xie, B., Long, J., Kuang, Y., Chen, X., Hou, M., Gao, J., Zhou, S., Fan, B., He, Y., et al. (2021). Interfacial laser-induced graphene enabling high-performance Liquid−Solid triboelectric nanogenerator. Adv. Mater. *33*, 2104290.

26. Liang, F., Chao, X., Yu, S., Gu, Y., Zhang, X., Wei, X., Fan, J., Tao, X., and Shou, D. (2022). An all-fabric droplet-based energy harvester with topology optimization. Adv. Energy Mater. *12*, 2102991.

27. Xi, Y., Hua, J., and Shi, Y. (2020). Noncontact triboelectric nanogenerator for human motion monitoring and energy harvesting. Nano Energy *69*, 104390.

28. Cho, S., Yun, Y., Jang, S., Ra, Y., Choi, J.H., Hwang, H.J., Choi, D., and Choi, D. (2020). Universal biomechanical energy harvesting from joint movements using a direction-switchable triboelectric nanogenerator. Nano Energy *71*, 104584.

29. Du, M., Cao, Y., Qu, X., Xue, J., Zhang, W., Pu, X., Shi, B., and Li, Z. (2022). Hybrid nanogenerator for biomechanical energy harvesting, motion state detection, and pulse sensing. Adv. Mater. Technol. 2101332. https://doi.org/10.1002/admt.202101332.

30. Ouyang, H., Liu, Z., Li, N., Shi, B., Zou, Y., Xie, F., Ma, Y., Li, Z., Li, H., Zheng, Q., et al. (2019). Symbiotic cardiac pacemaker. Nat. Commun. *10*, 1821.

31. Ryu, H., Park, H.-m., Kim, M.-K., Kim, B., Myoung, H.S., Kim, T.Y., Yoon, H.-J., Kwak, S.S., Kim, J., Hwang, T.H., et al. (2021). Self-rechargeable cardiac pacemaker system with triboelectric nanogenerators. Nat. Commun. *12*, 4374.

32. Su, Y., Chen, G., Chen, C., Gong, Q., Xie, G., Yao, M., Tai, H., Jiang, Y., and Chen, J. (2021). Self-powered respiration monitoring enabled by a triboelectric nanogenerator. Adv. Mater. *33*, 2101262.

33. Peng, X., Dong, K., Ning, C., Cheng, R., Yi, J., Zhang, Y., Sheng, F., Wu, Z., and Wang, Z.L. (2021). All-nanofiber self-powered skin-interfaced real-time respiratory monitoring system for obstructive sleep apnea-hypopnea syndrome diagnosing. Adv. Funct. Mater. *31*, 2103559.

34. Zheng, Q., Shi, B., Fan, F., Wang, X., Yan, L., Yuan, W., Wang, S., Liu, H., Li, Z., and Wang, Z.L. (2014). *In vivo* powering of pacemaker by breathing-driven implanted triboelectric nanogenerator. Adv. Mater. *26*, 5851–5856.

35. Sapra, N.V., Yang, K.Y., Vercruysse, D., Leedle, K.J., Black, D.S., England, R.J., Su, L., Trivedi, R., Miao, Y., Solgaard, O., et al. (2020). On-chip integrated laser-driven particle accelerator. Science *367*, 79–83.

36. Crowley-Milling, M.C. (1983). High-energy particle accelerators. Rep. Prog. Phys. *46*, 51–95.

37. Elserougi, A., Massoud, A.M., and Ahmed, S. (2017). A boost-inverter-based bipolar high-voltage pulse generator. IEEE Trans. Power Electron. *32*, 2846–2855.

38. Delshad, M.R., Rezanejad, M., and Sheikholeslami, A. (2017). A new modular bipolar high-voltage pulse generator. IEEE Trans. Ind. Electron. *64*, 1195–1203.

39. Beck, M.E., and Hersam, M.C. (2020). Emerging opportunities for electrostatic control in atomically thin devices. ACS Nano *14*, 6498–6518.

40. Meek, J.M., and Waterton, F.W. (1945). Measurement of high voltages. Nature *156*, 422–423.

41. Ahmad, V., Sobus, J., Greenberg, M., Shukla, A., Philippa, B., Pivrikas, A., Vamvounis, G.,

White, R., Lo, S.-C., and Namdas, E.B. (2020). Charge and exciton dynamics of OLEDs under high voltage nanosecond pulse: towards injection lasing. Nat. Commun. *11*, 4310.

42. Hokmabadi, M.P., Nye, N.S., El-Ganainy, R., Christodoulides, D.N., and Khajavikhan, M. (2019). Supersymmetric laser arrays. Science *363*, 623–626.

43. Hatzisymeon, M., Tataraki, D., Rassias, G., and Aggelopoulos, C.A. (2021). Novel combination of high voltage nanopulses and in-soil generated plasma micro-discharges applied for the highly efficient degradation of trifluralin. J. Hazard Mater. *415*, 125646.

44. Lukić, K., Vukušić, T., Tomašević, M., Ćurko, N., Gracin, L., and Kovačević Ganić, K. (2019). The impact of high voltage electrical discharge plasma on the chromatic characteristics and phenolic composition of red and white wines. Innov. Food Sci. Emerg. Technol. *53*, 70–77.

45. Duan, C., Han, J., Zhao, S., Gao, Z., Qiao, J., and Yan, G. (2018). The stripping effect of using high voltage electrical pulses breakage for waste printed circuit boards. Waste Manag. *77*, 603–610.

46. Wang, Q., Li, Y., Sun, D.-W., and Zhu, Z. (2018). Enhancing food processing by pulsed and high voltage electric fields: principles and applications. Crit. Rev. Food Sci. Nutr. *58*, 2285–2298.

47. Lei, R., Shi, Y., Ding, Y., Nie, J., Li, S., Wang, F., Zhai, H., Chen, X., and Wang, Z.L. (2020). Sustainable high-voltage source based on triboelectric nanogenerator with a charge accumulation strategy. Energy Environ. Sci. *13*, 2178–2190.

48. Yu, B., Yu, H., Huang, T., Wang, H., and Zhu, M. (2018). A biomimetic nanofiber-based triboelectric nanogenerator with an ultrahigh transfer charge density. Nano Energy *48*, 464–470.

49. Wang, Z.L. (2017). On Maxwell's displacement current for energy and sensors: the origin of nanogenerators. Mater. Today *20*, 74–82.

50. Dharmasena, R.D.I.G., Jayawardena, K.D.G.I., Mills, C.A., Deane, J.H.B., Anguita, J.V., Dorey, R.A., and Silva, S.R.P. (2017). Triboelectric nanogenerators: providing a fundamental framework. Energy Environ. Sci. *10*, 1801–1811.

51. Niu, S., Wang, S., Lin, L., Liu, Y., Zhou, Y.S., Hu, Y., and Wang, Z.L. (2013). Theoretical study of contact-mode triboelectric nanogenerators as an effective power source. Energy Environ. Sci. *6*, 3576–3583.

52. Niu, S., and Wang, Z.L. (2015). Theoretical systems of triboelectric nanogenerators. Nano Energy *14*, 161–192.

53. Niu, S., Liu, Y., Wang, S., Lin, L., Zhou, Y.S., Hu, Y., and Wang, Z.L. (2013). Theory of sliding-mode triboelectric nanogenerators. Adv. Mater. *25*, 6184–6193.

54. Niu, S., Liu, Y., Wang, S., Lin, L., Zhou, Y.S., Hu, Y., and Wang, Z.L. (2014). Theoretical investigation and structural optimization of single-electrode triboelectric nanogenerators. Adv. Funct. Mater. *24*, 3332–3340.

55. Jiang, T., Chen, X., Han, C.B., Tang, W., and Wang, Z.L. (2015). Theoretical study of rotary freestanding triboelectric nanogenerators. Adv. Funct. Mater. *25*, 2928–2938.

56. Zhang, X.S., Han, M.D., Wang, R.X., Zhu, F.Y., Li, Z.H., Wang, W., and Zhang, H.X. (2013). Frequency-multiplication high-output triboelectric nanogenerator for sustainably powering biomedical microsystems. Nano Lett. *13*, 1168–1172.

57. Feng, Y., Zhang, L., Zheng, Y., Wang, D., Zhou, F., and Liu, W. (2019). Leaves based triboelectric nanogenerator (TENG) and TENG tree for wind energy harvesting. Nano Energy *55*, 260–268.

58. Zhu, G., Pan, C., Guo, W., Chen, C.Y., Zhou, Y., Yu, R., and Wang, Z.L. (2012). Triboelectric-generator-driven pulse electrodeposition for micropatterning. Nano Lett. *12*, 4960–4965.

59. Wang, S., Zi, Y., Zhou, Y.S., Li, S., Fan, F., Lin, L., and Wang, Z.L. (2016). Molecular surface functionalization to enhance the power output of triboelectric nanogenerators. J. Mater. Chem. A Mater. *4*, 3728–3734.

60. Zhang, C., Mo, J., Fu, Q., Liu, Y., Wang, S., and Nie, S. (2021). Wood-cellulose-fiber-based functional materials for triboelectric nanogenerators. Nano Energy *81*, 105637.

61. Liu, Y., Mo, J., Fu, Q., Lu, Y., Zhang, N., Wang, S., and Nie, S. (2020). Enhancement of triboelectric charge density by chemical functionalization. Adv. Funct. Mater. *30*, 2004714.

62. Shin, S.H., Bae, Y.E., Moon, H.K., Kim, J., Choi, S.H., Kim, Y., Yoon, H.J., Lee, M.H., and Nah, J. (2017). Formation of triboelectric series via atomic-level surface functionalization for triboelectric energy harvesting. ACS Nano *11*, 6131–6138.

63. Han, S.A., Lee, K.H., Kim, T.-H., Seung, W., Lee, S.K., Choi, S., Kumar, B., Bhatia, R., Shin, H.-J., Lee, W.-J., et al. (2015). Hexagonal boron nitride assisted growth of stoichiometric Al2O3 dielectric on graphene for triboelectric nanogenerators. Nano Energy *12*, 556–566.

64. Huang, L.-B., Xu, W., Tian, W., Han, J.-C., Zhao, C.-H., Wu, H.-L., and Hao, J. (2020). Ultrasonic-assisted ultrafast fabrication of polymer nanowires for high performance triboelectric nanogenerators. Nano Energy *71*, 104593.

65. Song, W., Gan, B., Jiang, T., Zhang, Y., Yu, A., Yuan, H., Chen, N., Sun, C., and Wang, Z.L. (2016). Nanopillar arrayed triboelectric nanogenerator as a self-powered sensitive sensor for a sleep monitoring system. ACS Nano *10*, 8097–8103.

66. Dudem, B., Huynh, N.D., Kim, W., Kim, D.H., Hwang, H.J., Choi, D., and Yu, J.S. (2017). Nanopillar-array architectured PDMS-based triboelectric nanogenerator integrated with a windmill model for effective wind energy harvesting. Nano Energy *42*, 269–281.

67. Zhao, J., Li, H., Li, C., Zhang, Q., Sun, J., Wang, X., Guo, J., Xie, L., Xie, J., He, B., et al. (2018). MOF for template-directed growth of well-oriented nanowire hybrid arrays on carbon nanotube fibers for wearable electronics integrated with triboelectric nanogenerators. Nano Energy *45*, 420–431.

68. Lee, K.Y., Chun, J., Lee, J.H., Kim, K.N., Kang, N.R., Kim, J.Y., Kim, M.H., Shin, K.S., Gupta, M.K., Baik, J.M., and Kim, S.W. (2014). Hydrophobic sponge structure-based triboelectric nanogenerator. Adv. Mater. *26*, 5037–5042.

69. Cui, X., Zhao, T., Yang, S., Xie, G., Zhang, Z., Zhang, Y., Sang, S., Lin, Z.-H., Zhang, W., and Zhang, H. (2020). A spongy electrode-brush-structured dual-mode triboelectric nanogenerator for harvesting mechanical energy and self-powered trajectory tracking. Nano Energy *78*, 105381.

70. Bui, V., Zhou, Q., Kim, J., Oh, J., Han, K., Choi, H., Kim, S., and Oh, I. (2019). Treefrog toe pad-inspired micropatterning for high-power triboelectric nanogenerator. Adv. Funct. Mater. *29*, 1901638.

71. Seol, M.L., Woo, J.H., Lee, D.I., Im, H., Hur, J., and Choi, Y.K. (2014). Nature-replicated nano-in-micro structures for triboelectric energy harvesting. Small *10*, 3887–3894.

72. Chen, Y., Jie, Y., Wang, J., Ma, J., Jia, X., Dou, W., and Cao, X. (2018). Triboelectrification on natural rose petal for harvesting environmental mechanical energy. Nano Energy *50*, 441–447.

73. Li, X., Jiang, C., Yao, Y., Zhang, Q., Dai, S., Ying, Y., and Ping, J. (2021). Growth-controllable triboelectric nanogenerator based on surface-attached metal-organic framework layer on living leaf. Small *17*, 2103430.

74. Kim, J., Ryu, H., Lee, J.H., Khan, U., Kwak, S.S., Yoon, H., and Kim, S. (2020). High permittivity CaCu3Ti4O12 particle-induced internal polarization amplification for high performance triboelectric nanogenerators. Adv. Energy Mater. *10*, 2070040.

75. Feng, Y., Zheng, Y., Ma, S., Wang, D., Zhou, F., and Liu, W. (2016). High output polypropylene nanowire array triboelectric nanogenerator through surface structural control and chemical modification. Nano Energy *19*, 48–57.

76. Xia, S.-Y., Long, Y., Huang, Z., Zi, Y., Tao, L.-Q., Li, C.-H., Sun, H., and Li, J. (2022). Laser-induced graphene (LIG)-based pressure sensor and triboelectric nanogenerator towards high-performance self-powered measurement-control combined system. Nano Energy *96*, 107099.

77. Kim, S., Gupta, M.K., Lee, K.Y., Sohn, A., Kim, T.Y., Shin, K.-S., Kim, D., Kim, S.K., Lee, K.H., Shin, H.-J., et al. (2014). Transparent flexible graphene triboelectric nanogenerators. Adv. Mater. *26*, 3918–3925.

78. Cao, W., Ouyang, H., Xin, W., Chao, S., Ma, C., Li, Z., Chen, F., and Ma, M. (2020). A stretchable highoutput triboelectric nanogenerator improved by MXene liquid electrode with high electronegativity. Adv. Funct. Mater. *30*, 2004181.

79. Salauddin, M., Rana, S.M.S., Rahman, M.T., Sharifuzzaman, M., Maharjan, P., Bhatta, T., Cho, H., Lee, S.H., Park, C., Shrestha, K., et al.

(2022). Fabric-assisted MXene/silicone nanocomposite-based triboelectric nanogenerators for self-powered sensors and wearable electronics. Adv. Funct. Mater. *32*, 2107143.

80. Xiong, J., Cui, P., Chen, X., Wang, J., Parida, K., Lin, M.-F., and Lee, P.S. (2018). Skin-touch-actuated textile-based triboelectric nanogenerator with black phosphorus for durable biomechanical energy harvesting. Nat. Commun. *9*, 4280.

81. Gao, G., Wan, B., Liu, X., Sun, Q., Yang, X., Wang, L., Pan, C., and Wang, Z.L. (2018). Tunable tribotronic dual-gate logic devices based on 2D MoS2 and black phosphorus. Adv. Mater. *30*, 1705088.

82. Guo, Y., Cao, Y., Chen, Z., Li, R., Gong, W., Yang, W., Zhang, Q., and Wang, H. (2020). Fluorinated metal-organic framework as bifunctional filler toward highly improving output performance of triboelectric nanogenerators. Nano Energy *70*, 104517.

83. Rahman, M.T., Rana, S.S., Zahed, M.A., Lee, S., Yoon, E.-S., and Park, J.Y. (2022). Metal-organic framework-derived nanoporous carbon incorporated nanofibers for high-performance triboelectric nanogenerators and self-powered sensors. Nano Energy *94*, 106921.

84. Du, J., Yang, X., Duan, J., Wang, Y., and Tang, Q. (2020). Tailoring all-inorganic cesium lead halide perovskites for robust triboelectric nanogenerators. Nano Energy *70*, 104514.

85. Du, J., Duan, J., Yang, X., Wang, Y., Duan, Y., and Tang, Q. (2020). Charge boosting and storage by tailoring rhombus all-inorganic perovskite nanoarrays for robust triboelectric nanogenerators. Nano Energy *74*, 104845.

86. Li, Z., Xu, B., Han, J., Huang, J., and Chung, K.Y. (2021). Interfacial polarization and dual charge transfer induced high permittivity of carbon dots-based composite as humidity-resistant tribomaterial for efficient biomechanical energy harvesting. Adv. Energy Mater. *11*, 2101294.

87. Yu, A., Zhu, Y., Wang, W., and Zhai, J. (2019). Progress in triboelectric materials: toward high performance and widespread applications. Adv. Funct. Mater. *29*, 1900098.

88. Nie, J., Chen, X., and Wang, Z.L. (2018). Electrically responsive materials and devices directly driven by the high voltage of triboelectric nanogenerators. Adv. Funct. Mater. *29*, 1806351.

89. Yu, Y., and Wang, X. (2016). Chemical modification of polymer surfaces for advanced triboelectric nanogenerator development. Extreme Mechanics Letters *9*, 514–530.

90. Xu, L., Wu, H., Yao, G., Chen, L., Yang, X., Chen, B., Huang, X., Zhong, W., Chen, X., Yin, Z., and Wang, Z.L. (2018). Giant voltage enhancement via triboelectric charge supplement channel for self-powered electroadhesion. ACS Nano *12*, 10262–10271.

91. Wong, M., Xu, W., and Hao, J. (2019). Microplasma-discharge-based nitrogen fixation driven by triboelectric nanogenerator toward self-powered mechano-nitrogenous fertilizer supplier. Adv. Funct. Mater. *29*, 1904090.

92. Guo, H., Chen, J., Wang, L., Wang, A.C., Li, Y., An, C., He, J.-H., Hu, C., Hsiao, V.K.S., and Wang, Z.L. (2021). A highly efficient triboelectric negative air ion generator. Nat. Sustain. *4*, 147–153.

93. Wang, Z., Liu, W., Hu, J., He, W., Yang, H., Ling, C., Xi, Y., Wang, X., Liu, A., and Hu, C. (2020). Two voltages in contact-separation triboelectric nanogenerator: from asymmetry to symmetry for maximum output. Nano Energy *69*, 104452.

94. Wang, Z., Liu, J., Ma, F., Wang, J., Luo, Y., Fan, Y., Yuan, P., Zhang, P., Li, Q., Li, Q., and Xu, B. (2021). Ultrahigh electricity generation from low-frequency mechanical energy by efficient energy management. Breast Cancer Res. Treat. *188*, 441–447.

95. Chen, X., Pu, X., Jiang, T., Yu, A., Xu, L., and Wang, Z.L. (2017). Tunable optical modulator by coupling a triboelectric nanogenerator and a dielectric elastomer. Adv. Funct. Mater. *27*, 1603788.

96. Yang, D., Feng, Y., Wang, B., Liu, Y., Zheng, Y., Sun, X., Peng, J., Feng, M., and Wang, D. (2021). An asymmetric AC electric field of triboelectric nanogenerator for efficient water/oil emulsion separation. Nano Energy *90*, 106641.

97. Han, J., Feng, Y., Chen, P., Liang, X., Pang, H., Jiang, T., and Wang, Z.L. (2022). Wind-driven soft-contact rotary triboelectric nanogenerator based on rabbit Fur with high performance and durability for smart farming. Adv. Funct. Mater. *32*, 2108580.

98. Chen, P., An, J., Shu, S., Cheng, R., Nie, J., Jiang, T., and Wang, Z.L. (2021). Super-Durable, low-wear, and high-performance Fur-brush triboelectric nanogenerator for wind and water energy harvesting for smart agriculture. Adv. Energy Mater. *11*, 2003066.

99. Li, Q., Liu, W., Yang, H., He, W., Long, L., Wu, M., Zhang, X., Xi, Y., Hu, C., and Wang, Z.L. (2021). Ultra-stability high-voltage triboelectric nanogenerator designed by ternary dielectric triboelectrification with partial soft-contact and non-contact mode. Nano Energy *90*, 106585.

100. Li, X., Luo, J., Han, K., Shi, X., Ren, Z., Xi, Y., Ying, Y., Ping, J., and Wang, Z.L. (2022). Stimulation of ambient energy generated electric field on crop plant growth. Nat. Food *3*, 133–142.

101. Feng, H., Bai, Y., Qiao, L., Li, Z., Wang, E., Chao, S., Qu, X., Cao, Y., Liu, Z., Han, X., et al. (2021). An ultra-simple charge supplementary strategy for high performance rotary triboelectric nanogenerators. Small *17*, e2101430.

102. Chen, J., Wang, P., Li, J., Wang, C., Wang, J., Zhang, D., Peng, Y., Wang, B., and Wu, Z. (2022). Self-powered antifouling UVC pipeline sterilizer driven by the discharge stimuli based on the modified freestanding rotary triboelectric nanogenerator. Nano Energy *95*, 106969.

103. Lei, R., Shi, Y., Wang, X., Tao, X., Zhai, H., and Chen, X. (2021). Water purification system based on self-powered ozone production. Nano Energy *88*, 106230.

104. Luo, H., Gu, G., Shang, W., Zhang, W., Wang, T., Cui, P., Zhang, B., Guo, J., Cheng, G., and Du, Z. (2021). The water droplet with huge charge density excited by triboelectric nanogenerator for water sterilization. Nanotechnology *32*, 415404.

105. Bai, Y., Chen, S., Wang, H., Wang, E., Kong, X., Gai, Y., Qu, X., Li, Q., Xue, S., Guo, P., et al. (2022). Chemical warfare agents decontamination via air mircoplasma excited by a triboelectric nanogenerator. Nano Energy *95*, 106992.

106. Han, K., Luo, J., Feng, Y., Xu, L., Tang, W., and Wang, Z.L. (2020). Self-powered electrocatalytic ammonia synthesis directly from air as driven by dual triboelectric nanogenerators. Energy Environ. Sci. *13*, 2450–2458.

107. Han, K., Luo, J., Chen, J., Chen, B., Xu, L., Feng, Y., Tang, W., and Wang, Z.L. (2021). Self-powered ammonia synthesis under ambient conditions via N2 discharge driven by Tesla turbine triboelectric nanogenerators. Microsyst. Nanoeng. *7*, 7.

108. Gu, G., Gu, G., Wang, J., Yao, X., Ju, J., Cheng, G., and Du, Z. (2022). A water collection system with ultra-high harvest rate and ultra-low energy consumption by integrating triboelectric plasma. Nano Energy *96*, 107081.

109. Bai, Y., Xu, L., Lin, S., Luo, J., Qin, H., Han, K., and Wang, Z.L. (2020). Charge pumping strategy for rotation and sliding type triboelectric nanogenerators. Adv. Energy Mater. *10*, 2000605.

110. Yang, Z., Yang, Y., Liu, F., Li, B., Li, Y., Liu, X., Chen, J., Wang, C., Ji, L., Wang, Z.L., and Cheng, J. (2022). Thousandfold boosting instantaneous current of triboelectric nanogenerator based on decoupled charge pump and discharge tube. Nano Energy *98*, 107264.

111. Fu, S., He, W., Tang, Q., Wang, Z., Liu, W., Li, Q., Shan, C., Long, L., Hu, C., and Liu, H. (2022). An ultrarobust and high-performance rotational hydrodynamic triboelectric nanogenerator enabled by automatic mode switching and charge excitation. Adv. Mater. *34*, 2105882.

112. Nie, J., Ren, Z., Bai, Y., Shao, J., Jiang, T., Xu, L., Chen, X., and Wang, Z.L. (2019). Long distance transport of microdroplets and precise microfluidic patterning based on triboelectric nanogenerator. Adv. Mater. Technol. *4*, 1800300.

113. Li, C., Yin, Y., Wang, B., Zhou, T., Wang, J., Luo, J., Tang, W., Cao, R., Yuan, Z., Li, N., et al. (2017). Self-powered electrospinning system driven by a triboelectric nanogenerator. ACS Nano *11*, 10439–10445.

114. Han, C.B., Jiang, T., Zhang, C., Li, X., Zhang, C., Cao, X., and Wang, Z.L. (2015). Removal of particulate matter emissions from a vehicle using a self-powered triboelectric filter. ACS Nano *9*, 12552–12561.

115. Huo, H., Liu, F., Luo, Y., Gu, Q., Liu, Y., Wang, Z., Chen, R., Ji, L., Lu, Y., Yao, R., and Cheng, J. (2020). Triboelectric nanogenerators for

electro-assisted cell printing. Nano Energy 67, 104150.

116. Yang, H., Pang, Y., Bu, T., Liu, W., Luo, J., Jiang, D., Zhang, C., and Wang, Z.L. (2019). Triboelectric micromotors actuated by ultralow frequency mechanical stimuli. Nat. Commun. 10, 2309.

117. Zhao, L., Chen, K., Yang, F., Zheng, M., Guo, J., Gu, G., Zhang, B., Qin, H., Cheng, G., and Du, Z. (2019). The novel transistor and photodetector of monolayer MoS2 based on surface-ionic-gate modulation powered by a triboelectric nanogenerator. Nano Energy 62, 38–45.

118. Zhang, S., Guo, J., Liu, L., Ruan, H., Kong, C., Yuan, X., Zhang, B., Gu, G., Cui, P., Cheng, G., and Du, Z. (2022). The self-powered artificial synapse mechanotactile sensing system by integrating triboelectric plasma and gas-ionic-gated graphene transistor. Nano Energy 91, 106660.

119. Shan, C., He, W., Wu, H., Fu, S., Tang, Q., Wang, Z., Du, Y., Wang, J., Guo, H., and Hu, C. (2022). A high-performance bidirectional direct current TENG by triboelectrification of two dielectrics and local corona discharge. Adv. Energy Mater. 2200963. https://doi.org/10.1002/aenm.202200963.

120. He, W., Liu, W., Chen, J., Wang, Z., Liu, Y., Pu, X., Yang, H., Tang, Q., Yang, H., Guo, H., and Hu, C. (2020). Boosting output performance of sliding mode triboelectric nanogenerator by charge space-accumulation effect. Nat. Commun. 11, 4606.

121. Sun, J., Zhang, L., Li, Z., Tang, Q., Chen, J., Huang, Y., Hu, C., Guo, H., Peng, Y., and Wang, Z.L. (2021). A mobile and self-powered micro-flow pump based on triboelectricity driven electroosmosis. Adv. Mater. 33, e2102765.

122. Sun, W., Li, B., Zhang, F., Fang, C., Lu, Y., Gao, X., Cao, C., Chen, G., Zhang, C., and Wang, Z.L. (2021). TENG-Bot: triboelectric nanogenerator powered soft robot made of uni-directional dielectric elastomer. Nano Energy 85, 106012.

123. Qu, X., Ma, X., Shi, B., Li, H., Zheng, L., Wang, C., Liu, Z., Fan, Y., Chen, X., Li, Z., and Wang, Z.L. (2021). Refreshable braille display system based on triboelectric nanogenerator and dielectric elastomer. Adv. Funct. Mater. 31, 2006612.

124. Yu, J., Wei, X., Guo, Y., Zhang, Z., Rui, P., Zhao, Y., Zhang, W., Shi, S., and Wang, P. (2021). Self-powered droplet manipulation system for microfluidics based on triboelectric nanogenerator harvesting rotary energy. Lab Chip 21, 284–295.

125. Nie, J., Ren, Z., Shao, J., Deng, C., Xu, L., Chen, X., Li, M., and Wang, Z.L. (2018). Self-powered microfluidic transport system based on triboelectric nanogenerator and electrowetting technique. ACS Nano 12, 1491–1499.

126. Pang, H., Feng, Y., An, J., Chen, P., Han, J., Jiang, T., and Wang, Z.L. (2021). Segmented swing-structured Fur-based triboelectric nanogenerator for harvesting blue energy toward marine environmental applications. Adv. Funct. Mater. 31, 2106398.

127. Chen, P., An, J., Cheng, R., Shu, S., Berbille, A., Jiang, T., and Wang, Z.L. (2021). Rationally segmented triboelectric nanogenerator with a constant direct-current output and low crest factor. Energy Environ. Sci. 14, 4523–4532.

128. Fu, S., He, W., Wu, H., Shan, C., Du, Y., Li, G., Wang, P., Guo, H., Chen, J., and Hu, C. (2022). High output performance and ultra-durable DC output for triboelectric nanogenerator inspired by primary cell. Nano-Micro Lett. 14, 155.

129. Feng, Y., Zheng, Y., Zhang, G., Wang, D., Zhou, F., and Liu, W. (2017). A new protocol toward high output TENG with polyimide as charge storage layer. Nano Energy 38, 467–476.

130. Zhai, C., Chou, X., He, J., Song, L., Zhang, Z., Wen, T., Tian, Z., Chen, X., Zhang, W., Niu, Z., and Xue, C. (2018). An electrostatic discharge based needle-to-needle booster for dramatic performance enhancement of triboelectric nanogenerators. Appl. Energy 231, 1346–1353.

131. Liu, D., Yin, X., Guo, H., Zhou, L., Li, X., Zhang, C., Wang, J., and Wang, Z.L. (2019). A constant current triboelectric nanogenerator arising from electrostatic breakdown. Sci. Adv. 5, eaav6437.

132. Cheng, L., Xu, Q., Zheng, Y., Jia, X., and Qin, Y. (2018). A self-improving triboelectric nanogenerator with improved charge density and increased charge accumulation speed. Nat. Commun. 9, 3773.

133. Park, K.-I., Lee, M., Liu, Y., Moon, S., Hwang, G.-T., Zhu, G., Kim, J.E., Kim, S.O., Kim, D.K., Wang, Z.L., and Lee, K.J. (2012). Flexible nanocomposite generator made of BaTiO3 nanoparticles and graphitic carbons. Adv. Mater. 24, 2999–3004.

134. Park, H.-W., Huynh, N.D., Kim, W., Lee, C., Nam, Y., Lee, S., Chung, K.-B., and Choi, D. (2018). Electron blocking layer-based interfacial design for highly-enhanced triboelectric nanogenerators. Nano Energy 50, 9–15.

135. Yi, Z., Liu, D., Zhou, L., Li, S., Zhao, Z., Li, X., Wang, Z.L., and Wang, J. (2021). Enhancing output performance of direct-current triboelectric nanogenerator under controlled atmosphere. Nano Energy 84, 105864.

136. Wu, J., Xi, Y., and Shi, Y. (2020). Toward wear-resistive, highly durable and high performance triboelectric nanogenerator through interface liquid lubrication. Nano Energy 72, 104659.

137. He, W., Liu, W., Fu, S., Wu, H., Shan, C., Wang, Z., Xi, Y., Wang, X., Guo, H., Liu, H., and Hu, C. (2022). Ultrahigh performance triboelectric nanogenerator enabled by charge transmission in interfacial lubrication and potential decentralization design. Research 2022, 9812865.

138. Zhou, L., Liu, D., Zhao, Z., Li, S., Liu, Y., Liu, L., Gao, Y., Wang, Z.L., and Wang, J. (2020). Simultaneously enhancing power density and durability of sliding-mode triboelectric nanogenerator via interface liquid lubrication. Adv. Energy Mater. 10, 2002920.

139. Chung, S., Chung, J., Song, M., Kim, S., Shin, D., Lin, Z., Koo, B., Kim, D., Hong, J., and Lee, S. (2021). Nonpolar liquid lubricant submerged triboelectric nanogenerator for current amplification via direct electron flow. Adv. Energy Mater. 11, 2100936.

140. Kim, J., Cho, H., Han, M., Jung, Y., Kwak, S.S., Yoon, H., Park, B., Kim, H., Kim, H., Park, J., and Kim, S. (2020). Ultrahigh power output from triboelectric nanogenerator based on serrated electrode via spark discharge. Adv. Energy Mater. 10, 2002312.

141. Zhang, Q., Li, Y., Cai, H., Yao, M., Zhang, H., Guo, L., Lv, Z., Li, M., Lu, X., Ren, C., et al. (2021). A single-droplet electricity generator achieves an ultrahigh output over 100 V without pre-charging. Adv. Mater. 33, e2105761.

142. Xu, L., Bu, T.Z., Yang, X.D., Zhang, C., and Wang, Z.L. (2018). Ultrahigh charge density realized by charge pumping at ambient conditions for triboelectric nanogenerators. Nano Energy 49, 625–633.

143. Li, Y., Zhao, Z., Liu, L., Zhou, L., Liu, D., Li, S., Chen, S., Dai, Y., Wang, J., and Wang, Z.L. (2021). Improved output performance of triboelectric nanogenerator by fast accumulation process of surface charges. Adv. Energy Mater. 11, 2100050.

144. Li, Y., Zhao, Z., Gao, Y., Li, S., Zhou, L., Wang, J., and Wang, Z.L. (2021). Low-cost, environmentally friendly, and high-performance triboelectric nanogenerator based on a common waste material. ACS Appl. Mater. Interfaces 13, 30776–30784.

145. Long, L., Liu, W., Wang, Z., He, W., Li, G., Tang, Q., Guo, H., Pu, X., Liu, Y., and Hu, C. (2021). High performance floating self-excited sliding triboelectric nanogenerator for micro mechanical energy harvesting. Nat. Commun. 12, 4689.

146. Liu, W., Wang, Z., Wang, G., Liu, G., Chen, J., Pu, X., Xi, Y., Wang, X., Guo, H., Hu, C., and Wang, Z.L. (2019). Integrated charge excitation triboelectric nanogenerator. Nat. Commun. 10, 1426.

147. Chen, X., Jiang, T., and Wang, Z.L. (2017). Modeling a dielectric elastomer as driven by triboelectric nanogenerator. Appl. Phys. Lett. 110, 033505.

148. Chen, S., Pang, Y., Yuan, H., Tan, X., and Cao, C. (2020). Smart soft actuators and grippers enabled by self-powered tribo-skins. Advanced Materials Technologies 5.

149. Chen, X., Jiang, T., Yao, Y., Xu, L., Zhao, Z., and Wang, Z.L. (2016). Stimulating acrylic elastomers by a triboelectric nanogenerator - toward self-powered electronic skin and artificial muscle. Adv. Funct. Mater. 26, 4906–4913.

150. Chen, X., Wu, Y., Yu, A., Xu, L., Zheng, L., Liu, Y., Li, H., and Lin Wang, Z. (2017). Self-powered modulation of elastomeric optical grating by using triboelectric nanogenerator. Nano Energy 38, 91–100.

151. Zhang, C., Wang, H., Guan, S., Guo, Z., Zheng, X., Fan, Y., Wang, Y., Qu, T., Zhao, Y., Chen, A., et al. (2019). Self-powered optical switch based on triboelectrification-triggered liquid crystal alignment for wireless sensing. Adv. Funct. Mater. 29, 1808633.

152. Chen, Y.-H., Lin, P.-Y., Wang, T.-W., Tiwari, N., Lin, S.-C., Wu, H.-S., Choi, D., Wu, W., Choi, D., Hsiao, Y.-C., and Lin, Z.H. (2021). Dynamics of electrically driven cholesteric liquid crystals by triboelectrification and their application in self-powered information securing and vision correcting. ACS Energy Lett. *6*, 3185–3194.

153. Wang, J., Meng, C., Gu, Q., Tseng, M.C., Tang, S.T., Kwok, H.S., Cheng, J., and Zi, Y. (2020). Normally transparent tribo-induced smart window. ACS Nano *14*, 3630–3639.

154. Ke, Y., Chen, J., Lin, G., Wang, S., Zhou, Y., Yin, J., Lee, P.S., and Long, Y. (2019). Smart windows: electro-thermo-mechano-photochromics, and beyond. Adv. Energy Mater. *9*, 1970153.

155. Wang, J., Liu, P., Meng, C., Kwok, H.S., and Zi, Y. (2021). Tribo-induced smart reflector for ultrasensitive self-powered wireless sensing of air flow. ACS Appl. Mater. Interfaces *13*, 21450–21458.

156. Liu, H., Guo, Z.H., Xu, F., Jia, L., Pan, C., Wang, Z.L., and Pu, X. (2021). Triboelectric-optical responsive cholesteric liquid crystals for self-powered smart window, E-paper display and optical switch. Sci. Bull. *66*, 1986–1993.

157. Fang, H., Li, Q., He, W., Li, J., Xue, Q., Xu, C., Zhang, L., Ren, T., Dong, G., Chan, H.L.W., et al. (2015). A high performance triboelectric nanogenerator for self-powered non-volatile ferroelectric transistor memory. Nanoscale *7*, 17306–17311.

158. Chen, X., Iwamoto, M., Shi, Z., Zhang, L., and Wang, Z.L. (2015). Self-powered trace memorization by conjunction of contact-electrification and ferroelectricity. Adv. Funct. Mater. *25*, 739–747.

159. Lee, J.-H., Hinchet, R., Kim, T.Y., Ryu, H., Seung, W., Yoon, H.-J., and Kim, S.-W. (2015). Control of skin potential by triboelectrification with ferroelectric polymers. Adv. Mater. *27*, 5553–5558.

160. Zheng, L., Wu, Y., Chen, X., Yu, A., Xu, L., Liu, Y., Li, H., and Wang, Z.L. (2017). Self-powered electrostatic actuation systems for manipulating the movement of both microfluid and solid objects by using triboelectric nanogenerator. Adv. Funct. Mater. *27*, 1606408.

161. Nie, J., Jiang, T., Shao, J., Ren, Z., Bai, Y., Iwamoto, M., Chen, X., and Wang, Z.L. (2018). Motion behavior of water droplets driven by triboelectric nanogenerator. Appl. Phys. Lett. *112*, 183701.

162. Zhou, J., Tao, Y., Liu, W., Sun, H., Wu, W., Song, C., Xue, R., Jiang, T., Jiang, H., and Ren, Y. (2021). Self-powered AC electrokinetic microfluidic system based on triboelectric nanogenerator. Nano Energy *89*, 106451.

163. Sun, X., Feng, Y., Wang, B., Liu, Y., Wu, Z., Yang, D., Zheng, Y., Peng, J., Feng, M., and Wang, D. (2021). A new method for the electrostatic manipulation of droplet movement by triboelectric nanogenerator. Nano Energy *86*, 106115.

164. Wu, C., Tetik, H., Cheng, J., Ding, W., Guo, H., Tao, X., Zhou, N., Zi, Y., Wu, Z., Wu, H., et al. (2019). Electrohydrodynamic jet printing driven by a triboelectric nanogenerator. Adv. Funct. Mater. *29*, 1901102.

165. Liu, Y., Wen, J., Chen, B., Zheng, M., Liu, D., Liu, Y., Tang, W., Liu, J., Nan, D., and Wang, Z.L. (2020). Electro-blown spinning driven by cylindrical rotating triboelectric nanogenerator and its applications for fabricating nanofibers. Appl. Mater. Today *19*, 100631.

166. Han, Y., Zou, J., Li, Z., Wang, W., Jie, Y., Ma, J., Tang, B., Zhang, Q., Cao, X., Xu, S., and Wang, Z.L. (2018). Si@void@C nanofibers fabricated using a self-powered electrospinning system for lithium-ion batteries. ACS Nano *12*, 4835–4843.

167. Chen, S., Gao, C., Tang, W., Zhu, H., Han, Y., Jiang, Q., Li, T., Cao, X., and Wang, Z. (2015). Self-powered cleaning of air pollution by wind driven triboelectric nanogenerator. Nano Energy *14*, 217–225.

168. Gu, G.Q., Han, C.B., Lu, C.X., He, C., Jiang, T., Gao, Z.L., Li, C.J., and Wang, Z.L. (2017). Triboelectric nanogenerator enhanced nanofiber air filters for efficient particulate matter removal. ACS Nano *11*, 6211–6217.

169. Gu, G.Q., Han, C.B., Tian, J.J., Jiang, T., He, C., Lu, C.X., Bai, Y., Nie, J.H., Li, Z., and Wang, Z.L. (2018). Triboelectric nanogenerator enhanced multilayered antibacterial nanofiber air filters for efficient removal of ultrafine particulate matter. Nano Res. *11*, 4090–4101.

170. Feng, Y., Ling, L., Nie, J., Han, K., Chen, X., Bian, Z., Li, H., and Wang, Z.L. (2017). Self-powered electrostatic filter with enhanced photocatalytic degradation of formaldehyde based on built-in triboelectric nanogenerators. ACS Nano *11*, 12411–12418.

171. Mo, J., Zhang, C., Lu, Y., Liu, Y., Zhang, N., Wang, S., and Nie, S. (2020). Radial piston triboelectric nanogenerator-enhanced cellulose fiber air filter for self-powered particulate matter removal. Nano Energy *78*, 105357.

172. Bai, Y., Han, C.B., He, C., Gu, G.Q., Nie, J.H., Shao, J.J., Xiao, T.X., Deng, C.R., and Wang, Z.L. (2018). Washable multilayer triboelectric air filter for efficient particulate matter PM2.5Removal. Adv. Funct. Mater. *28*, 1706680.

173. Yoon, H.-J., Kim, D.-H., Seung, W., Khan, U., Kim, T.Y., Kim, T., and Kim, S.-W. (2019). 3D-printed biomimetic-villus structure with maximized surface area for triboelectric nanogenerator and dust filter. Nano Energy *63*, 103857.

174. Liu, G., Nie, J., Han, C., Jiang, T., Yang, Z., Pang, Y., Xu, L., Guo, T., Bu, T., Zhang, C., and Wang, Z.L. (2018). Self-powered electrostatic adsorption face mask based on a triboelectric nanogenerator. ACS Appl. Mater. Interfaces *10*, 7126–7133.

175. Cheng, Y., Wang, C., Zhong, J., Lin, S., Xiao, Y., Zhong, Q., Jiang, H., Wu, N., Li, W., Chen, S., et al. (2017). Electrospun polyetherimide electret nonwoven for bi-functional smart face mask. Nano Energy *34*, 562–569.

176. He, X., Zou, H., Geng, Z., Wang, X., Ding, W., Hu, F., Zi, Y., Xu, C., Zhang, S.L., Yu, H., et al. (2018). A hierarchically nanostructured cellulose fiber-based triboelectric nanogenerator for self-powered healthcare products. Adv. Funct. Mater. *28*, 1805540.

177. Ghatak, B., Banerjee, S., Ali, S.B., Bandyopadhyay, R., Das, N., Mandal, D., and Tudu, B. (2021). Design of a self-powered triboelectric face mask. Nano Energy *79*, 105387.

178. Wang, N., Feng, Y., Zheng, Y., Zhang, L., Feng, M., Li, X., Zhou, F., and Wang, D. (2021). New hydrogen bonding enhanced polyvinyl alcohol based self-charged medical mask with superior charge retention and moisture resistance performances. Adv. Funct. Mater. *31*, 2009172.

179. Cheng, J., Ding, W., Zi, Y., Lu, Y., Ji, L., Liu, F., Wu, C., and Wang, Z.L. (2018). Triboelectric microplasma powered by mechanical stimuli. Nat. Commun. *9*, 3733.

180. Liu, F., Liu, Y., Lu, Y., Wang, Z., Shi, Y., Ji, L., and Cheng, J. (2019). Electrical analysis of triboelectric nanogenerator for high voltage applications exampled by DBD microplasma. Nano Energy *56*, 482–493.

181. Yang, F., Zheng, M., Zhao, L., Guo, J., Zhang, B., Gu, G., Cheng, G., and Du, Z. (2019). The high-speed ultraviolet photodetector of ZnO nanowire Schottky barrier based on the triboelectric-nanogenerator-powered surface-ionic-gate. Nano Energy *60*, 680–688.

182. Wang, C., Li, X., Wang, L., Liu, G., Nie, B., Qiu, Y., Fan, B., Yan, C., Chen, X., Tian, H., et al. (2021). Metal micropatterning by triboelectric spark discharge. Adv. Funct. Mater. *32*, 2109265.

183. Zheng, M., Yang, F., Guo, J., Zhao, L., Jiang, X., Gu, G., Zhang, B., Cui, P., Cheng, G., and Du, Z. (2020). Cd(OH)2@ZnO nanowires thin-film transistor and UV photodetector with a floating ionic gate tuned by a triboelectric nanogenerator. Nano Energy *73*, 104808.

184. Luo, J., Han, K., Wu, X., Cai, H., Jiang, T., Zhou, H., and Wang, Z.L. (2021). Self-powered mobile sterilization and infection control system. Nano Energy *88*, 106313.

185. Li, A., Zi, Y., Guo, H., Wang, Z.L., and Fernández, F.M. (2017). Triboelectric nanogenerators for sensitive nano-coulomb molecular mass spectrometry. Nat. Nanotechnol. *12*, 481–487.

186. Bernier, M.C., Li, A., Winalski, L., Zi, Y., Li, Y., Caillet, C., Newton, P., Wang, Z.L., and Fernández, F.M. (2018). Triboelectric nanogenerator (TENG) mass spectrometry of falsified antimalarials. Rapid Commun. Mass Spectrom. *32*, 1585–1590.

187. Cho, S., Hanif, Z., Yun, Y., Khan, Z.A., Jang, S., Ra, Y., Lin, Z.-H., La, M., Park, S.J., and Choi, D. (2021). Triboelectrification-driven microbial inactivation in a conductive cellulose filter for affordable, portable, and efficient water sterilization. Nano Energy *88*, 106228.

188. Chiu, C.-M., Ke, Y.-Y., Chou, T.-M., Lin, Y.-J., Yang, P.-K., Wu, C.-C., and Lin, Z.-H. (2018). Self-powered active antibacterial clothing through hybrid effects of nanowire-enhanced electric field electroporation and controllable hydrogen peroxide generation. Nano Energy *53*, 1–10.

189. Huo, Z.Y., Kim, Y.J., Suh, I.Y., Lee, D.M., Lee, J.H., Du, Y., Wang, S., Yoon, H.J., and Kim, S.W. (2021). Triboelectrification induced self-powered microbial disinfection using nanowire-enhanced localized electric field. Nat. Commun. *12*, 3693.

190. Zhao, C., Feng, H., Zhang, L., Li, Z., Zou, Y., Tan, P., Ouyang, H., Jiang, D., Yu, M., Wang, C., et al. (2019). Highly efficient *in vivo* cancer therapy by an implantable magnet triboelectric nanogenerator. Adv. Funct. Mater. *29*, 1970285.

191. Liu, Z., Nie, J., Miao, B., Li, J., Cui, Y., Wang, S., Zhang, X., Zhao, G., Deng, Y., Wu, Y., et al. (2019). Self-powered intracellular drug delivery by a biomechanical energy-driven triboelectric nanogenerator. Adv. Mater. *31*, e1807795.

192. Tian, J., Feng, H., Yan, L., Yu, M., Ouyang, H., Li, H., Jiang, W., Jin, Y., Zhu, G., Li, Z., and Wang, Z.L. (2017). A self-powered sterilization system with both instant and sustainable anti-bacterial ability. Nano Energy *36*, 241–249.

193. Yang, C., Yang, G., Ouyang, Q., Kuang, S., Song, P., Xu, G., Poenar, D.P., Zhu, G., Yong, K.-T., and Wang, Z.L. (2019). Nanowire-array-based gene electro-transfection system driven by human-motion operated triboelectric nanogenerator. Nano Energy *64*, 103901.

194. Liu, Z., Liang, X., Liu, H., Wang, Z., Jiang, T., Cheng, Y., Wu, M., Xiang, D., Li, Z., Wang, Z.L., and Li, L. (2020). High-throughput and self-powered electroporation system for drug delivery assisted by microfoam electrode. ACS Nano *14*, 15458–15467.

195. Liu, L., Yang, X., Zhao, L., Hong, H., Cui, H., Duan, J., Yang, Q., and Tang, Q. (2021). Nodding duck structure multi-track directional freestanding triboelectric nanogenerator toward low-frequency ocean wave energy harvesting. ACS Nano *15*, 9412–9421.

196. Cheng, J., Zhang, X., Jia, T., Wu, Q., Dong, Y., and Wang, D. (2022). Triboelectric nanogenerator with a seesaw structure for harvesting ocean energy. Nano Energy *102*, 107622.

197. Feng, L., Liu, G., Guo, H., Tang, Q., Pu, X., Chen, J., Wang, X., Xi, Y., and Hu, C. (2018). Hybridized nanogenerator based on honeycomb-like three electrodes for efficient ocean wave energy harvesting. Nano Energy *47*, 217–223.